

Statistical Molecule Counting in Super-Resolution Fluorescence Microscopy: Towards Quantitative Nanoscopy

T. Staudt* T. Aspelmeier* C. Geisler[†] A. Egner[†] A. Munk*

May 26, 2022

Abstract

Super-resolution microscopy is rapidly gaining importance as an analytical tool in the life sciences. A compelling feature is the ability to label biological units of interest with fluorescent markers in living cells and to observe them with considerably higher resolution than conventional microscopy permits. The images obtained this way, however, lack an absolute intensity scale in terms of numbers of fluorophores observed. We provide an elaborate model to estimate this information from the raw data. To this end we model the entire process of photon generation in the fluorophore, their passage through the microscope, detection and photo electron amplification in the camera, and extraction of time series from the microscopic images. At the heart of these modeling steps is a careful description of the fluorophore dynamics by a novel hidden Markov model that operates on two time scales (HTMM). Besides the fluorophore number, information about the kinetic transition rates of the fluorophore's internal states is also inferred during estimation. We comment on computational issues that arise when applying our model to simulated or measured fluorescence traces and illustrate our methodology on simulated data.

Keywords: fluorescence, molecule counting, super-resolution microscopy, quantitative nanoscopy, biophysics and computational biology, inhomogeneous hidden Markov models, statistical thinning.

AMS 2010 Subject Classification: primary 62M05; secondary 60J10, 62P10, 62P35

1 Introduction

During the past decades cell biology has undergone a profound transition, shifting its character from qualitative work about cell activity to increasingly quantitative methods to study the role of individual proteins for signaling and transport. This trend was crucially supported by the advancement of super-resolution microscopy (nanoscopy) techniques, which have since become

*Institute for Mathematical Stochastics, Georg-August-University of Göttingen

[†]Laser-Laboratorium Göttingen e.V.

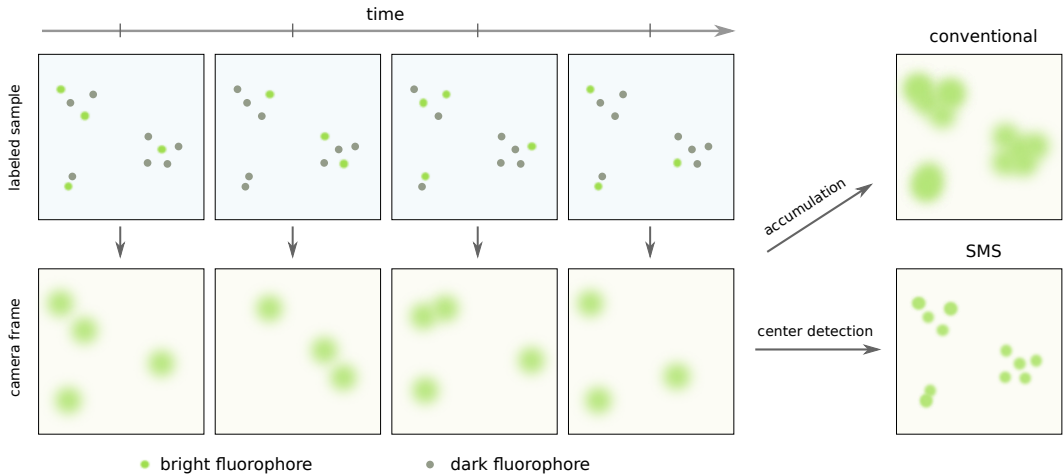


Figure 1: Principle of single-marker-switching microscopy. By exciting a biological sample that is labeled with fluorophores (top row) via a suitable laser, a temporal series of frames capturing fluorescent activity is recorded (bottom row). In each frame, only a sparse selection of fluorophores emits photons (green circles). The recorded images are blurry because of inevitable diffraction effects. Still, the center positions of the individual diffraction limited spots can be determined with higher precision due to spatial sparsity. This can be used to create a pointillistic nanoscopy image with superior resolution as compared to conventional fluorescence microscopy, where the photons emitted by all fluorophores would be recorded at the same time.

an indispensable tool for modern biomedical research [14, 5, 13, 28]. While previous imaging methods for cellular structures were either limited due to a lack of resolution (like conventional light microscopy) or due to their invasiveness (like X-ray or electron microscopy), fluorescence nanoscopy enables high-resolution imaging of living cells to the nanometer scale without the necessity to prepare samples in ways that prohibit natural biochemical activity. The limits of super-resolution microscopy, both in principle and application, are still being explored and progress unfolds at a considerable pace [15, 2].

By now, a multitude of methodologies to overcome the diffraction barrier through the usage of switchable fluorescent probes have been proposed. Several common forms of super-resolution microscopy are based on the concept of single-marker-switching (SMS), like PALM [5], STORM [27], GSDIM [10], or variations thereof [16, 8, 30]. The principle idea of SMS nanoscopy is to record a series of diffraction limited fluorescence images (frames) in which only a small number of (randomly selected) fluorophores emits photons during each exposure. This way, spatially close molecules are effectively separated in time. Using the detected fluorophore positions from all frames, a pointillistic image with superior resolution can be created (see Figure 1). Even though it is possible to localize individual fluorescent probes within this scheme, deriving quantitative information from these images is difficult. This poses a fundamental challenge for the application of SMS microscopy in quantitative biology.

In order to obtain exact fluorophore numbers from fluorescence images, several methods have been proposed in recent years, see [20, 26, 29]. They either rely on the detection of switching

events of single fluorophores or on counting the number of steps during photobleaching. While these methods have been successfully applied to count 50 fluorophores and more in specific circumstances [20, 29], they can be prone to errors when misidentifying switching events or bleaching steps due to the sophisticated blinking behavior of fluorophores. These issues become particularly pressing in the presence of many fluorophores within a diffraction limited region and when the fluorophore kinetics connected with bleaching and switching are fast in comparison to the image acquisition rate.

In this report, we document a novel method to estimate the number of fluorophores that contribute to a region of interest (ROI) on a series of fluorescence microscopy images. Contrary to established methods, no step identification (which usually involves the choice of fluorescence levels or rate thresholds and relies on bleaching or switching) is necessary. This becomes possible by carefully modeling the whole physical imaging process from photon generation in the fluorophore to signal amplification in the CCD camera. Our approach makes use of the full history of the recorded intensity information, and it heavily relies on exploiting temporal correlations in the signal. Fundamental for this is an accurate description of the fluorophore behavior, for which we employ a novel hidden Markov model that operates on two distinct time scales: it separates the *fast dynamics* that govern the emission of single photons during the exposure from the *slow dynamics* that describe fluorophore kinetics for states with dwell times longer than a single frame. Although our Markov model is time-inhomogeneous, estimation of the fluorophore number (and other kinetic parameters) can be performed by applying the maximum likelihood principle to the pseudo log-likelihood, which is a simplified expression for the model's total likelihood. We exploit certain spectral properties of the model to this end. Remarkably, the quantity of interest in our problem – the fluorophore number – is a feature of the initial state of the model. Due to bleaching of fluorophores, this information is lost in the asymptotic behavior. Our method has been thoroughly tested on experimental super-resolution images of DNA origami [19].

The article is organized as follows. In section 2, we provide an overview of the single modeling steps that contribute to our total model for the fluorescent time traces, and we briefly describe how we estimate the fluorophore number with it. Section 3 then contains a detailed treatment of the fluorophore dynamics. We formulate the hidden two-timescale Markov model (HTMM) that is based on the description of fluorescent molecules as Markov chains, possibly acting on different timescales with different transition rates. In particular, we derive expressions for the expectation and (co-)variance of the number of emitted photons in each frame, and provide results about spectral properties of the transition matrix which are useful for computational purposes (Appendix B and C). In section 4, we investigate how the number of emitted photons is transformed through (i) statistical thinning in the microscope and (ii) processing and amplification in the detector. For reasons of clarity, the central notation that is introduced in sections 3 and 4 is surveyed in Table 1 on page 26. In section 5, we then introduce the pseudo log-likelihood and comment on numerical issues for maximum likelihood estimation based on it. Finally, in section 6, we specialize our general model to fit the quantum physical state space of the commonly used fluorophore Alexa 647.

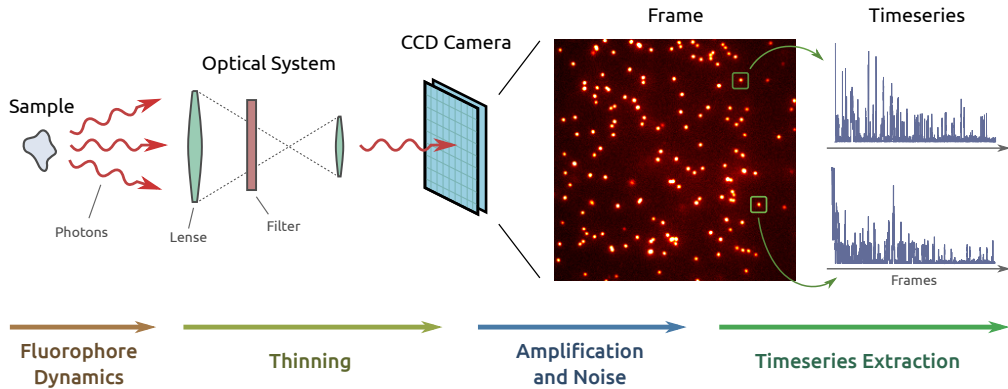


Figure 2: Overview of the modeling steps. During exposure, fluorophores within a labeled biological sample emit photons due to laser excitation. With a certain probability, these photons pass through the microscope (optical system) and are registered by a CCD camera. Over the course of the experiment, a series of camera frames is recorded. Summing up the intensities over a region of interest (ROI, green boxes) for each image yields a time series that captures the fluorescent activity in the respective ROI.

2 Modeling and Estimation

Super-resolution microscopy with single marker switching (SMS) relies on a series of fluorescence microscopy images, or frames, with only a small fraction of active fluorophores per image. This way, spatially close fluorophores are separated in time since they are unlikely to emit photons simultaneously. The resulting frames are used to localize the marker molecules with a superior precision on the nanometer scale [28]. The imaging is affected by the quantum physical behavior of the fluorophore, which leads to *switching* and *bleaching*, and by a series of subsequent manipulations of the emitted photons until they are detected by the camera and transformed to digital values [1]. Each step in this chain (depicted in Figure 2) modifies the original signal – photons emitted by the fluorophore – in a characteristic way and has to be taken into account. In the following, we present an outline of our approach to estimate the fluorophore number based on time traces extracted from a series of T camera images. More detailed considerations follow in subsequent sections.

Single fluorophore. Fluorophore dynamics is successfully modeled by Markov chains [21, 24]. The states of these chains roughly correspond to quantum physical states of the molecule (see Remark 1 below), which can exhibit very diverse lifetimes. The respective transition rates are governed by quantum mechanical kinetics that sensitively depend on the biochemical properties of the fluorophore's neighbourhood in the sample. Two of the states have a distinguished role in our model: the *bright* state, in which absorption and emission of photons is possible, and the *bleached* state, in which dyes have irreversibly lost their fluorescence functionality. Additionally, a number of temporary *dark* states, which, e.g., correspond to triplet or redox states of the fluorophore [31], are usually necessary for a faithful description.

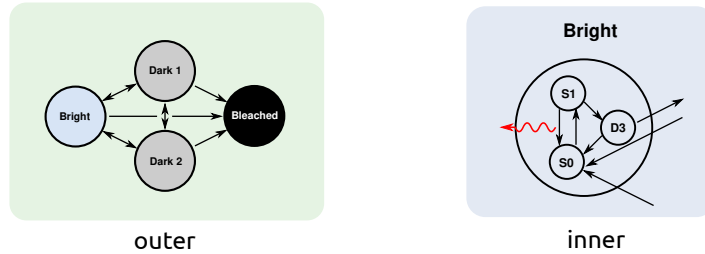


Figure 3: Exemplary inner and outer models that are used to describe the dynamics of the fluorophore Alexa 647 (see [19]). The wiggling red arrow indicates that transitions from the singlet state S_1 to the ground state S_0 cause the emission of a photon. The state D_3 is a short-lived dark state.

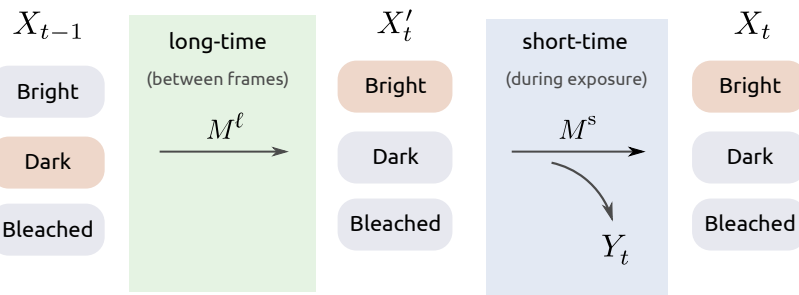


Figure 4: Single fluorophore model. At time $t - 1$, the fluorophore can be in one of several distinct outer states X_{t-1} . When transitioning from X_{t-1} to X_t , we apply the long-time matrix M^ℓ to describe the dynamics that takes place between separate frames, and then apply the short-time matrix M^s for the effects of the fast dynamics on the outer state during exposure. In the latter step, the fluorophore emits a number Y_t of photons in frame t .

Remark 1: In Markov chains, states with the same transition rates can be combined into a single state without losing the Markov property (see appendix A for details). A reasonable fluorophore model does therefore not have to include every possible quantum physical state explicitly (like fine-structured rotational and vibrational substates). Rather, it only has to capture classes of states with similar dwell times and transition behavior. The number of such classes can be estimated from the data.

The phenomenon of fluorophores jumping between the bright and temporary dark states is denoted as *blinking* or *switching*. In our generic model for fluorescence, we finely resolve the fast dynamics inherent to the bright state, like single photon emissions, and model it as a Markov chain in its own right. This gives rise to a description that operates on two different time scales: a fast *inner model* that runs during the exposure time, and a slow *outer model* that captures states that are expected to persist over several frames. Figure 3 depicts our choice of states for the fluorophore Alexa 647, which we investigate more detailed in Section 6.

Let X'_t denote the outer state of the fluorophore directly before the t -th exposure, and let X_t denote its state after the exposure. The transition from X_{t-1} to X_t is depicted in Figure 4. It is modeled through applying one step of the outer dynamics on X_{t-1} , which yields X'_t , and then running the inner model, which changes X'_t to X_t , and which also yields a number Y_t of emitted photons during frame t . The distribution of Y_t depends on both X'_t and X_t . A complete description of our model for fluorophore dynamics is therefore given by a transition matrix M^ℓ for the long-time step, a matrix M^s for the short-time step, and the distribution $p_{xx'}$ of Y_t conditioned on $X_t = x$ and $X'_t = x'$, which we assume to be stationary. The combined chain

$$(X_0, X'_1, X_1, X'_2, \dots)$$

of outer states is an inhomogeneous Markov chain with alternating transition matrices M^ℓ and M^s , while the individual chains $(X_t)_t$ and $(X'_t)_t$ are homogeneous with transition matrices $M^s M^\ell$ and $M^\ell M^s$, respectively.

In experiment, the states X_t and X'_t cannot be observed directly. We only obtain outputs of the measurement device (e.g., a CCD camera) generated through the Y_t emitted photons. This makes our ansatz a hidden Markov model. In Section 3, we derive the generating function of the process $Y = (Y_t)_{t=1}^T$ and obtain its expectation μ and the covariance Σ , which are eventually used to estimate the number of fluorophores in section 5.

Remark 2 (notation): We refer to the model outlined above as hidden two-timescale Markov model, or HTMM. The observable part of this model, Y_t , denotes the number of photons that are emitted in the time interval between X'_t and X_t . One can therefore think of X'_t as the state X_{t^-} directly prior to X_t , and Y_t as an observation that accumulates from t^- to t .

Microscope and camera. Photons emitted by fluorescent dyes are directed randomly and may fail to enter the microscope, such that they are lost for the experiment. In addition, a photon may be absorbed by lenses, filters, or mirrors within the optical path. Consequently, each emitted photon has a probability $p_c < 1$ to reach the camera. When it reaches the camera, the position of the photon on the CCD sensor is randomized due to diffraction: light originating from a point source is spread to a blurred spot on the detector interface. From the viewpoint of classical physics, where light is modeled as a wave of electromagnetic radiation, this blurring is described by a convolution of the light intensity distribution with a nonnegative point spread function h (see [11, 6] for the underlying physics and [1] for a treatment in the context of statistics). In the quantum mechanical interpretation of light as photons, $h(z)$ denotes the probability that a photon emitted at the origin of the sample incides at pixel z on the detector, which leads to a multinomial distribution of incident photons to pixel locations. When the photon arrives at a pixel z , it is absorbed with a certain probability p_a and a so-called photo electron, i.e., an electron ejected from the detector material due to energy transfer from the photon, is released. The total chance for a photon to reach the detector at any pixel and be absorbed is denoted by $p_d = p_c p_a$.

We call a region R on the image that captures the blurred spot created by one (or several close-by) fluorophores a region of interest (ROI). The total number Y'_t of detected photons in R is given by

$$Y'_t = \sum_{z \in R} Y'_{t,z}$$

where $Y'_{t,z}$ is the number of photons detected at pixel $z \in R$. Since we assume that the electrical circuits underlying individual pixels are identical in their properties, we can ignore the spatial distribution of photons within one ROI and work with $Y'_t \sim \text{Bin}(Y_t, p_d)$ directly. This amounts to a binomial thinning of Y_t [12].

Since the electrical charge of a photo electron is too small to be detected reliably, cameras employ an electron multiplying system that operates stochastically [25, 17]. Let \mathcal{D} denote the distribution for the number of electrons after amplification of the incoming electron in the CCD. Then the final camera output value \tilde{Y}_t , when summed over R , is given by

$$\tilde{Y}_t = c \sum_{k=1}^{Y'_t} U_{t,k} + \epsilon_t + o, \quad (1)$$

with $U_{t,k} \sim \mathcal{D}$ i.i.d. for all t and k . The constant factor $c > 0$ results due to the analog-to-digital conversion of the accumulated electron charge in the pixels, and the random variables ϵ_t collect different contributions of inevitable additional randomness – like background photons, thermal electrons in the electronics, or readout noise. Additionally, a constant positive offset o is added to the camera output to avoid noise induced fluctuations into the negative domain.

Multiple fluorophores. Each fluorophore in the bright state produces a diffraction-limited spot during exposure, as seen in the frame shown in Figure 2. The major difficulty for estimating the number of fluorophores reliably results from the fact that several fluorophores can contribute to the same spot if their mutual distance is small and if they are bright simultaneously. The core contribution of this report is to use the information from a temporal series of frames to estimate the total number m of fluorophores that are present in a given region of interest R .

Remark 3: The unknown number m of fluorophores is the major quantity of interest to be estimated in a single ROI. By combining estimates for m from different ROIs, one can obtain quantitative information on the spatial fluorophore density in the entire image.

A crucial assumption that we use to model multi-fluorophore systems is *statistical independence*, i.e., that no (relevant) physical interactions between the single fluorophores take place. We also assume that all m fluorophores are *identical* in their physical behavior, meaning that they can be described by a common fluorophore model with a common set of parameters. Then, the total number of emitted photons is given by the sum of m independent copies Y_t^1, \dots, Y_t^m of the process Y_t ,

$$Y_t^{(m)} = \sum_{k=1}^m Y_t^k. \quad (2)$$

Similarly, the time series obtained by summing the CCD values over the region R is composed of m independent versions $\tilde{Y}_t^1, \dots, \tilde{Y}_t^m$ of \tilde{Y}_t . Therefore, the total signal we observe is encoded in the process

$$\tilde{Y}_t^{(m)} = \sum_{k=1}^m \tilde{Y}_t^k.$$

Remark 4: The assumptions of independence and identical distribution are approximations that are justified for many typical experimental situations. Still, they can be violated, e.g., if the spatial distance of neighbouring fluorophores is very small (< 10 nm). Then, interactions like FRET (Förster Resonance Energy Transmission) become likely. The experimental study [19] highlights that our model indeed produces inconsistent results in this case.

Estimation. Our objective is to estimate m from a realization y of the process $\tilde{Y}^{(m)} = (\tilde{Y}_t^{(m)})_t$. Besides m , there are several other parameters that may have to be estimated, like the transition rates in the HTMM, or the initial distribution of the outer state. These parameters depend sensitively on details of the experimental setting, like the fluorophore type, the biochemical conditions in the sample, or the applied laser wavelengths and intensities. Some of these properties may vary from ROI to ROI. Furthermore, different types of fluorophores may even require different inner or outer models. This poses an interesting problem in model selection – which we will, however, not address in this report.

Since the number of unknown parameters, which we call γ for the moment, is typically small (e.g., at most 16 for our Alexa 647 model with three dark states, see Section 6), it is near at hand to employ maximum likelihood estimation. However, the computation of the MLE requires that we can evaluate the log-likelihood $l_y(\gamma)$ of the full model, which is unfeasible for two reasons: first, the number of terms in $l_y(\gamma)$ turns out to be overwhelming even for a moderate number T of frames; and secondly, we lack information about how the signal is transformed in the camera, since manufacturers usually only provide information about the first two moments of the camera-statistics \mathcal{D} . We therefore choose an approach that is based on approximating $\tilde{Y}^{(m)}$ by a Gaussian process with the same expectation $\mu = \mu(\gamma)$ and covariance $\Sigma = \Sigma(\gamma)$ as $\tilde{Y}^{(m)}$. This leads to the *pseudo log-likelihood*

$$\tilde{l}_y(\gamma) = -\frac{1}{2} \left[(y - \mu) \Sigma^{-1} (y - \mu) + \log \det \Sigma \right],$$

and parameter estimation reduces to maximizing $\tilde{l}_y(\gamma)$. This is still challenging but becomes numerically feasible. In particular, we have fewer degrees of freedom: for Alexa 647, only 11 (compared to 16) independent parameters are necessary to fully describe μ and Σ , since the first two moments do not rely on all transition probabilities of the HTMM individually. In section 5, we address a number of subtleties that come along with this approach, like nonlinear constraints on the parameter space.

We stress that other methods of estimation may certainly be of interest. In particular, a Bayesian approach becomes feasible when prior knowledge on parameters is available. We do, however, not pursue this issue further in this report and content ourselves to (pseudo) maximum likelihood based statistical analysis.

3 Fluorophore Dynamics

The dynamics of fluorophores is at the heart of our model for the imaging process in Figure 2. Due to the i.i.d. assumption when modeling multiple fluorophores (see Remark 4), this effectively amounts to modeling a single fluorophore. In this section, we will treat the short-time dynamics as a “black box” with as few assumptions as is necessary. Only later, when we specialize the model to the fluorophore Alexa 647 in Section 6, we elaborate on a concrete inner model. As a guidance for the derivations that follow, consulting Table 1 on page 26 might prove helpful, which summarizes the relevant notation that is introduced in this and the next section.

Fluorophore model. The outer state space of a fluorophore is described by one bright and $r \in \mathbb{N}$ dark states, including the bleached one. See Figure 3 for an example. We name the state space \mathcal{S} and denote its elements by $x \in \mathcal{S} = \{0, \dots, r\}$, with $x = 0$ being the bright and $x = r$ being the bleached state. On \mathcal{S} , we consider two coupled time-discrete Markov chains $(X_t)_{t=0}^T$ and $(X'_t)_{t=1}^T$, where $T \in \mathbb{N}$ is the number of frames. The evolution of X_t and X'_t is given by the (stationary) transition matrices M^ℓ and M^s , where

$$M_{x'x}^\ell = \mathbb{P}(X'_t = x' \mid X_{t-1} = x) \quad \text{and} \quad M_{xx'}^s = \mathbb{P}(X_t = x \mid X'_t = x') \quad (3a)$$

for $x, x' \in \mathcal{S}$. We interpret X'_t as state of the fluorophore directly before exposure in frame t , and X_t as state directly after exposure (see Remark 2 and Figure 4). The full transition matrix for X_t is given by

$$M = M^s M^\ell. \quad (3b)$$

The transition of the fluorophore from X'_t to X_t during exposure is governed by the inner model, which also determines the number Y_t of photons that are emitted in the corresponding frame. We characterize the photon statistics of the inner model by the conditional distributions

$$p_{xx'}(y) = \mathbb{P}(Y_t = y \mid X_t = x, X'_t = x') \quad (4)$$

for $y \in \mathbb{N}_0$, which we assume to be time-stationary. The probabilities in (4) are collected in the matrix $P(y) = (p_{xx'})_{x, x' \in \mathcal{S}}$. We furthermore use the symbol $\nu = (\nu_x)_{x \in \mathcal{S}}$ to denote the initial distribution, i.e., the distribution of X_0 . In total, specification of M^s , M^ℓ , P , and ν completely defines a single-fluorophore model.

Definition 1: Any observable process $Y = (Y_t)_t$ as constructed above, with conditional distributions P in (4), transition matrices M^s and M^ℓ defined in (3), and initial (hidden) distribution ν , is denoted as hidden two-timescale Markov model, or HTMM.

Lemma 1: The likelihood of an HTTM under observation of a time series $y = (y_t)_{t=1}^T$ is

$$l_y(M^s, M^\ell, P, v) = \sum_{x \in \mathcal{S}^{T+1}} \left(\prod_{t=1}^T \sum_{x' \in \mathcal{S}} p_{x_t x'}(y_t) M_{x_t x'}^s M_{x' x_{t-1}}^\ell \right) v_{x_0}, \quad (5)$$

where the outer sum covers all tuples $x = (x_0, x_1, \dots, x_T) \in \mathcal{S}^{T+1}$.

Proof. A single transition step under observation of $Y_t = y$ photons is described by

$$\mathbb{P}(Y_t = y, X_t = x \mid X_{t-1} = z) = \sum_{x' \in \mathcal{S}} p_{xx'}(y) M_{xx'}^s M_{x' z}^\ell,$$

and the probability to observe the full time series $(y_t)_{t=1}^T$ can be written as

$$\mathbb{P}(Y_t = y_t \text{ for all } t) = \sum_{x \in \mathcal{S}^{T+1}} \left(\prod_{t=1}^T \mathbb{P}(Y_t = y_t, X_t = x_t \mid X_{t-1} = x_{t-1}) \right) v_{x_0}.$$

Combining these two equations yields the stated result. \square

Remark 5: The outer sum in equation (5) contains $(r+1)^{T+1}$ terms, and we are not aware of a way to significantly simplify the expression under general circumstances. Since there is at least one dark outer state (meaning $r \geq 1$) and the number T of frames for SMS microscopy is often well above 1000, it is impossible to directly evaluate the likelihood l_y numerically ($2^{1000} > 10^{300}$).

Remark 6: We will eventually extend the HTMM in Definition 1 by (i) the generalization to multiple i.i.d. fluorophores, and (ii) the additional statistical modeling of the imaging process (see Section 4). These enhanced models will for convenience also be referred to as HTMMs, since the context usually clarifies which specific fluorophore model is meant.

Model restrictions. We introduce several restrictions on our model in order to reflect physical fluorophore properties and to make the analysis of (5) viable. The most evident constraint is that the bleached state $x = r$ acts as an absorbing state for both M^s and M^ℓ . We also assume that the fluorophore can leave the bright state $x = 0$ only during application of the inner model. Conversely, we suppose that a fluorophore that is not in its bright state is unaffected by the inner model. With these restrictions in place, M^ℓ and M^s can be brought in the respective

parametric forms

$$M^\ell = \begin{pmatrix} 1 & q_{01} & \cdots & q_{0(r-1)} & 0 \\ 0 & q_{11} & \cdots & q_{1(r-1)} & 0 \\ \vdots & \vdots & \ddots & \vdots & \vdots \\ 0 & q_{(r-1)1} & \cdots & q_{(r-1)(r-1)} & 0 \\ 0 & q_{r1} & \cdots & q_{r(r-1)} & 1 \end{pmatrix} \quad \text{and} \quad M^s = \begin{pmatrix} q_{00} & 0 & \cdots & 0 & 0 \\ q_{10} & 1 & \cdots & 0 & 0 \\ \vdots & \vdots & \ddots & \vdots & \vdots \\ q_{(r-1)0} & 0 & \cdots & 1 & 0 \\ q_{r0} & 0 & \cdots & 0 & 1 \end{pmatrix}, \quad (6)$$

where we defined transition probabilities $q_{xz} \in [0, 1]$ for $x \in \mathcal{S}$ and $z \in \mathcal{S} \setminus \{r\}$. The restrictions also imply that no photons are emitted if the exposure starts in a non-bright state, meaning that $p_{xx'}(0) = 1$ for $x' \neq 0$. In contrast, if the exposure begins in the bright state $x' = 0$, the fluorophore will produce photons and may switch to any other state $x \in \mathcal{S}$ until the end of the exposure.

An additional assumption that is required to make the model analytically tractable is that the distribution p_{x0} does not depend on the final state x if the fluorophore exits the bright state. This means that

$$p_{x0} = p_{10} \quad \text{if } x > 0. \quad (7)$$

Remark 7: Condition (7) can be understood as assuming a common “exit state” in the inner model that is the only possibility for the fluorophore to become dark during exposure. From this state, it can then jump to all dark states of the outer model as soon as the frame ends. Note that this exit state does not have to correspond to a (single) physical state: it could cover several states with similar exit conditions (see Remark 1 in this context).

Under these constraints, the conditional distributions of the photon statistics defined in (4) read

$$P(y) = \begin{pmatrix} p_{00}(y) & \delta(y) & \cdots & \delta(y) \\ p_{10}(y) & \delta(y) & \cdots & \delta(y) \\ \vdots & \vdots & \ddots & \vdots \\ p_{10}(y) & \delta(y) & \cdots & \delta(y) \end{pmatrix}, \quad (8)$$

where δ denotes the Dirac measure with point mass 1 on $y = 0$. Fluorophore models that satisfy conditions (6) and (8) are collected in the set \mathcal{F}^s of (physical) single-fluorophore models.

Generating function. Even when exploiting the additional constraints for \mathcal{F}^s , the process $Y = (Y_t)_t$ of emitted photons remains very complex. In particular, it is hard to use the HTMM for straightforward inference. Maximum likelihood estimation, e.g., is impossible for real world datasets due to the prohibitive expense of calculating the likelihood, see Remark 5. We can, however, use the moment generating function of Y and the specific structure of \mathcal{F}^s to calculate expressions for the expectations $\mu_t = \mathbb{E}[Y_t]$ and the covariance Σ ,

$$\Sigma_{tt'} = \mathbb{E}[(Y_t - \mathbb{E}Y_t)(Y_{t'} - \mathbb{E}Y_{t'})],$$

where $t, t' = 1, \dots, T$. These moments carry relevant information and allow recovering the number of fluorophores in case of multiple molecules (see Section 5). For preparation, we first look at the moment generating matrix $G(s)$ associated to $P(y)$ and find

$$G(s) = \begin{pmatrix} G_{00}(s) & 1 & \cdots & 1 \\ G_{10}(s) & 1 & \cdots & 1 \\ \vdots & \vdots & \ddots & \vdots \\ G_{10}(s) & 1 & \cdots & 1 \end{pmatrix}, \quad (9)$$

where $G_{00}(s) = \mathbb{E}[e^{sY_t} | X_t = X'_t = 0]$ and $G_{10}(s) = \mathbb{E}[e^{sY_t} | X_t = 1, X'_t = 0]$. Then, we define the auxiliary matrix

$$H(s) = (G(s) \circ M^s) M^\ell, \quad (10)$$

where \circ denotes the entry-wise (Hadamard) product. In the following, we will only consider inner models for which the expectations G_{00} and G_{10} exist and are finite in some vicinity $(-\epsilon, \epsilon)$ of zero for $\epsilon > 0$. In particular, this implies that all derivatives of H exist at $s = 0$ [9].

Lemma 2: The moment generating function G_Y of the process Y is given by

$$G_Y(\tau) = (1, \dots, 1) H(\tau_T) \cdots H(\tau_1) v \quad (11)$$

for $\tau = (\tau_1, \dots, \tau_T) \in (-\epsilon, \epsilon)^T$.

Proof. Consulting equation (5) and definition (10), calculation shows

$$\begin{aligned} G_Y(\tau) &= \mathbb{E} \left[\exp \left(\sum_{t=1}^T \tau_t Y_t \right) \right] \\ &= \sum_{y \in \mathbb{N}_0^T} \sum_{x \in \mathcal{S}^{T+1}} \left(\prod_{t=1}^T \sum_{x' \in \mathcal{S}} p_{x_t x'}(y_t) e^{\tau_t y_t} M_{x_t x'}^s M_{x' x_{t-1}}^\ell \right) v_{x_0} \\ &= (1, \dots, 1) H(\tau_T) \cdots H(\tau_1) v \end{aligned}$$

for the moment generating function. \square

Moments of the inner model. Before we derive the expectation and covariance of Y by differentiating equation (11), we introduce three parameters θ_1 , θ_2 , and θ_3 that describe the photon emission statistics p_{00} and p_{10} up to second order. The first parameter θ_1 describes the expected number of photons emitted during the frame if the fluorophore was in the bright state initially,

$$\theta_1 = \mathbb{E}[Y_t | X'_t = 0] = \sum_{x \in \mathcal{S}} q_{x0} \mathbb{E}[Y_t | X'_t = 0, X_t = x], \quad (12a)$$

where we used that $q_{x0} = M_{x0}^s = \mathbb{P}(X_t = x \mid X'_t = 0)$ by definition. The second parameter θ_2 quantifies the contribution to the expectation θ_1 if the fluorophore not only starts the frame in the bright state but also stays there,

$$\theta_2 = \frac{q_{00} \mathbb{E}[Y_t \mid X'_t = X_t = 0]}{\theta_1}. \quad (12b)$$

Finally, we capture the conditioned variance of Y_t given $X'_t = 0$ via the parameter θ_3 ,

$$\theta_3 = \frac{\text{Var}[Y_t \mid X'_t = 0]}{\theta_1^2} - \frac{1}{\theta_1}. \quad (12c)$$

This parameter can be viewed as the excess relative variance with respect to a Poisson distribution: if $Y_t \mid X_t = 0$ was distributed Poissonian, then $\theta_3 = 0$. A Poissonian statistics is often assumed as an approximation for the photon emission of fluorophores, but corrections may be necessary for accurate results [1].

Remark 8: The parameters $\theta = (\theta_1, \theta_2, \theta_3)$ clearly depend on the inner model choice and are usually related to the entries of the short-time transition matrix M^s . For example, we show in Section 6 that θ_2 is fully determined by q_{00} in the inner model that we use for the fluorophore Alexa 647.

Expectation. In order to derive analytical expressions for the expectation and covariance, we will assume that the transition matrix $M = M^s M^\ell$ is diagonalizable and has eigenvalues $\lambda_0, \dots, \lambda_r \in \mathbb{C}$. We argue that this assumption is no significant restriction, since the stochastic matrices that are not diagonalizable form a null set – see Lemma 9 in appendix B for details. We thus write

$$M = V \Lambda V^{-1}, \quad (13)$$

where $\Lambda = \text{diag}(\lambda_0, \dots, \lambda_r)$ and where V is a matrix containing the eigenvectors of M as columns. Due to the absorbing nature of the bleached state $x = r$, we can assume that $\lambda_r = 1$ with eigenvector $(0, 0, \dots, 1)^T$, which hence constitutes the last column of V .

Theorem 1: Assume that the Markov matrix M for a single-fluorophore model in \mathcal{F}^s is diagonalizable like in (13). Then the expectation value μ_t of the number Y_t of photons emitted by the fluorophore at time $t = 1, \dots, T$ is

$$\mu_t = \theta_1 \sum_{x \in \mathcal{S}} \alpha_x \lambda_x^{t-1}, \quad (14)$$

where the coefficients α_x for $x \in \mathcal{S}$ are defined by

$$\alpha_x = V_{0x} \frac{\lambda_x}{q_{00}} \sum_{z \in \mathcal{S}} V_{xz}^{-1} \nu_z. \quad (15)$$

Proof. Upon differentiating the moment generating function $G_Y(\tau)$ in equation (11) with respect to τ_t , one obtains the expectation value of Y_t ,

$$\begin{aligned}\mu_t &= \mathbb{E}[Y_t] = \frac{\partial G_Y(\tau)}{\partial \tau_t} \Big|_{\tau=0} \\ &= (1, \dots, 1) H(\tau_T) \cdots H(\tau_{t+1}) H'(\tau_t) H(\tau_{t-1}) \cdots H(\tau_1) v_0 \Big|_{\tau=0} \\ &= (1, \dots, 1) H'(0) M^{t-1} v_0.\end{aligned}\tag{16}$$

The last line follows from $(1, \dots, 1) H(0) = (1, \dots, 1)$, which holds since $H(0) = M^s M^\ell = M$ is a probability matrix. The derivative of H is given by

$$H'(s) = (G'(s) \circ M^s) M^\ell,$$

where G' is the derivative of the generating matrix G defined in equation (9). Due to the particular form of M^ℓ , M^s , and $G(s)$, see equations (6) and (9), it follows with definition (12a) of θ_1 that

$$\begin{aligned}(1, \dots, 1) H'(0) &= \theta_1 (1, 0, \dots, 0) M^\ell \\ &= \frac{\theta_1}{q_{00}} (1, 0, \dots, 0) M.\end{aligned}\tag{17}$$

Here, we used that the respective first rows of M^ℓ and M only differ by the factor q_{00} . Combining equations (16) and (17), we can express the expectation by

$$\mu_t = \frac{\theta_1}{q_{00}} \sum_{z \in \mathcal{S}} M_{0z}^t v_z.\tag{18}$$

If we now use representation (13) of M , we find

$$\begin{aligned}\mu_t &= \frac{\theta_1}{q_{00}} \sum_{z \in \mathcal{S}} (V \Lambda^t V^{-1})_{0z} v_z \\ &= \frac{\theta_1}{q_{00}} \sum_{x \in \mathcal{S}} \left(V_{0x} \sum_{z \in \mathcal{S}} V_{xz}^{-1} v_z \right) \lambda_x^t \\ &= \theta_1 \sum_{x \in \mathcal{S}} \alpha_x \lambda_x^{t-1},\end{aligned}\tag{19}$$

which proves the theorem. \square

In order to express the covariance of Y later, we will need the expectation value μ_t^0 of Y_t on the condition that the fluorophore was in the bright state at the beginning of the experiment. This corresponds to the case $v = (1, 0, \dots, 0)$. According to equation (18), we thus find

$$\mu_t^0 = \mathbb{E}[Y_t | X_0 = 0] = \frac{\theta_1}{q_{00}} (M^t)_{00}.\tag{20}$$

Under assumption (13) of diagonalizability for M , Theorem 1 lets us write

$$\mu_t^0 = \theta_1 \sum_{x \in \mathcal{S}} \alpha_x^0 \lambda_x^{t-1},$$

where the coefficients α_x^0 are given by equation (15) with $\nu = (1, 0, \dots, 0)$,

$$\alpha_x^0 = \frac{\lambda_x}{q_{00}} V_{0x} V_{x0}^{-1}. \quad (21)$$

These auxiliary coefficients α_x^0 can be related to α_x . If $\nu_0 = 1$, then $\alpha_x^0 = \alpha_x$ by definition. If $\nu_0 < 1$, we can plug $\nu' = \frac{1}{1-\nu_0}(0, \nu_1, \dots, \nu_r)$ in equation (15) and define

$$\alpha_x^1 = \frac{\lambda_x}{q_{00}} V_{0x} \sum_{z \in \mathcal{S}} V_{xz}^{-1} \nu'_z, \quad (22)$$

which allows us to decompose α_x as

$$\alpha_x = \nu_0 \alpha_x^0 + (1 - \nu_0) \alpha_x^1.$$

This way of splitting up the model parameters has the advantage that a simple set of constraints for α_x^0 and α_x^1 arises (see Lemma 3 below).

Spectral properties and parameter constraints. The eigenvalues λ_x and coefficients α_x in Theorem 1 can in general be complex-valued. To estimate these parameters numerically, however, it is beneficial to assume real eigenvalues and eigenvectors of M . In Appendix C, we provide some criteria that guarantee $\lambda_x \in [0, 1]$ for $r \leq 3$. In summary, (i) real and (ii) positive eigenvalues are ensured if the diagonal values of the transition matrix M are (i) diverse and (ii) large enough. Usually, both of these assumptions are physically reasonable: the diagonal values are diverse if the outer states of the fluorophore exhibit diverse live times, and they are large if the outer states are on average stable over several frames. Under the restriction $\lambda_x \in [0, 1]$ on the spectrum of M , equation (14) states that the expected number μ_t of emitted photons is the superposition of exponential decays with timescales determined by λ_x .

Furthermore, note that the coefficients α_x are implicitly constrained by their definition in equation (15). First,

$$\alpha_r = 0$$

is enforced due to $V_{0r} = 0$. This is physically expected as fluorophores in the bleached state do not emit photons. Secondly, summing over $x \in \mathcal{S}$ in (15) shows

$$\sum_{x \in \mathcal{S}} \alpha_x = \frac{1}{q_{00}} \sum_{z \in \mathcal{S}} M_{0z} \nu_z = (1, q_{01}, \dots, q_{0(r-1)}, 0) \nu. \quad (23)$$

Similarly, we find the relation

$$\sum_{x \in \mathcal{S}} \frac{\alpha_x}{\lambda_x} = \frac{\nu_0}{q_{00}}. \quad (24)$$

by dividing equation (15) by λ_x and again summing over $x \in \mathcal{S}$. Applying the last three equations to the coefficients α_x^0 and α_x^1 , defined in (21) and (22), yields a set of simple constraints.

Lemma 3: We have $\alpha_r^0 = \alpha_r^1 = 0$. Furthermore, it holds that

$$\sum_{x \in \mathcal{S}} \alpha_x^0 = 1 \quad \text{and} \quad \sum_{x \in \mathcal{S}} \frac{\alpha_x^0}{\lambda_x} = \frac{1}{q_{00}}, \quad (25a)$$

$$0 \leq q_{00} \sum_{x \in \mathcal{S}} \alpha_x^1 \leq 1 \quad \text{and} \quad \sum_{x \in \mathcal{S}} \frac{\alpha_x^1}{\lambda_x} = 0. \quad (25b)$$

Proof. The first statement holds due to $V_{0r} = 0$. The relations in (25a) follow from equation (23) and (24) for $v = (1, 0, \dots, 0)$. Constraint (25b) follows similarly if we take into account that v' is a probability vector with $v'_0 = 0$. \square

Covariance. We next look at the covariance matrix Σ of the process Y , which can be obtained from the second derivatives of the moment generating function G_Y .

Theorem 2: Under assumption (13), the covariance matrix Σ of the process $Y = (Y_t)_{t=1}^T$ is

$$\Sigma_{tt} = (\theta_1(\theta_3 + 1) + 1 - \mu_t) \mu_t, \quad (26a)$$

$$\Sigma_{tt'} = \left[\left(\theta_2 - q_{00} \frac{1 - \theta_2}{1 - q_{00}} \right) \mu_{t-t'}^0 + \frac{1 - \theta_2}{1 - q_{00}} \mu_{t-t'+1}^0 - \mu_t \right] \mu_{t'}, \quad (26b)$$

on the diagonal and off-diagonal with $t > t'$, respectively.

Proof. One can derive the entries of the covariance matrix for times $t, t' = 1, \dots, T$ by

$$\Sigma_{tt'} = \frac{\partial^2 G_Y(\tau)}{\partial \tau_t \partial \tau_{t'}} \Big|_{\tau=0} - \mu_t \mu_{t'}. \quad (27)$$

We first address the diagonal with $t = t'$. In this case, we can proceed similarly to equation (16) and find

$$\Sigma_{tt} = (1, \dots, 1) H''(0) M^{t-1} v - \mu_t^2. \quad (28)$$

Again, one can exploit the special forms of M^ℓ , M^s , and $G(\tau)$ to obtain

$$\begin{aligned} (1, \dots, 1) H''(0) &= \theta_1^2(\theta_3 + 1/\theta_1 + 1) (1, 0, \dots, 0) M^\ell \\ &= \frac{\theta_1^2(\theta_3 + 1/\theta_1 + 1)}{q_{00}} (1, 0, \dots, 0) M, \end{aligned}$$

where we used the relation between θ_1 , θ_3 , and the second moments $G''_{00}(0)$ and $G''_{10}(0)$. Consulting equations (16) and (17) now reveals

$$(1, \dots, 1) H''(0) M^{t-1} v = \theta_1(\theta_3 + 1/\theta_1 + 1) \mu_t.$$

Plugging this expression in equation (28) shows result (26a).

We next consider the off-diagonal entries with $t > t'$. Applying equation (27) yields

$$\Sigma_{tt'} = (1, \dots, 1) H'(0) M^{t-t'-1} H'(0) M^{t'-1} v - \mu_t \mu_{t'}.$$

Since $H'(0) = (G'(0) \circ M^s) M^\ell$, and since only the first column of $G'(0)$ is unequal to 0, we find that

$$\begin{aligned} (1, \dots, 1) H'(0) M^{t-t'-1} H'(0) &= \beta \theta_1 (1, 0, \dots, 0) M^\ell \\ &= \beta \frac{\theta_1}{q_{00}} (1, 0, \dots, 0) M, \end{aligned}$$

where β is given by

$$\begin{aligned} \beta &= \frac{1}{\theta_1} (1, \dots, 1) H'(0) M^{t-t'-1} (G'(0) \circ M^s) (1, 0, \dots, 0)^T \\ &= \frac{1}{q_{00}} (1, 0, \dots, 0) M^{t-t'} (G'(0) \circ M^s) (1, 0, \dots, 0)^T. \end{aligned} \quad (29)$$

We employed equation (17) for the second equality. Remarkably, we can now use the same reasoning as for the expectation and the diagonal entries before, and we find that

$$\Sigma_{tt'} = \beta \mu_{t'} - \mu_t \mu_{t'}. \quad (30)$$

This reduces the problem to resolving β . We begin by looking at the first column of $G'(0) \circ M^s$, which is given by

$$(G'(0) \circ M^s) \begin{pmatrix} 1 \\ 0 \\ \vdots \\ 0 \end{pmatrix} = \begin{pmatrix} G'_{00}(0) q_{00} \\ G'_{10}(0) q_{10} \\ \vdots \\ G'_{r0}(0) q_{r0} \end{pmatrix} = \theta_1 \theta_2 \begin{pmatrix} 1 \\ 0 \\ \vdots \\ 0 \end{pmatrix} + \theta_1 \frac{1 - \theta_2}{1 - q_{00}} \begin{pmatrix} 0 \\ q_{10} \\ \vdots \\ q_{r0} \end{pmatrix}. \quad (31)$$

Here, we used that $G'_{xx'}(0) = \mathbb{E}[Y_t \mid X_t = x, X'_t = x']$ and applied definitions (12a–b) of θ_1 and θ_2 . The assumption of a common exit state in the fast model (see Remark 7), which ensures that $G_{10} = G_{x0}$ for all $x \geq 1$, is crucial for this step. Equation (31) decomposes β into two parts, and we accordingly write

$$\beta = \theta_2 \beta_1 + \frac{1 - \theta_2}{1 - q_{00}} \beta_2. \quad (32)$$

We address β_1 first. By inserting the first term of (31) in (29), we find that

$$\beta_1 = \frac{\theta_1}{q_{00}} (1, 0, \dots, 0) M^{t-t'} (1, 0, \dots, 0)^T = \frac{\theta_1}{q_{00}} (M^{t-t'})_{00} = \mu_{t-t'}^0,$$

where definition (20) of μ_t^0 was applied. In order to express β_2 , we first note that the respective first columns of the two matrices M^s and M are equal, namely $(q_{00}, \dots, q_{r0})^T$. Thus, we can express q_{x0} in terms of the diagonal decomposition (13) of M ,

$$q_{x0} = M_{x0} = (V \Lambda V^{-1})_{x0}.$$

We then harness the auxiliary calculation

$$\sum_{z=1}^r V_{xz}^{-1} q_{z0} = \sum_{z=1}^r V_{xz}^{-1} (V \Lambda V^{-1})_{z0} = \lambda_x V_{x0}^{-1} - q_{00} V_{x0}^{-1},$$

which can be verified by straightforward computation, and arrive at

$$\begin{aligned} \beta_2 &= \frac{\theta_1}{q_{00}} (1, 0, \dots, 0) M^{t-t'} (0, q_{10}, \dots, q_{r0})^T \\ &= \frac{\theta_1}{q_{00}} (1, 0, \dots, 0) V \Lambda^{t-t'} V^{-1} (0, q_{10}, \dots, q_{r0})^T \\ &= \frac{\theta_1}{q_{00}} (1, 0, \dots, 0) \left(M^{t-t'+1} - q_{00} M^{t-t'} \right) (1, 0, \dots, 0)^T. \end{aligned}$$

Making use of the definition (20) of μ_t^0 , we conclude $\beta_2 = \mu_{t-t'+1}^0 - q_{00} \mu_{t-t'}^0$. Together with $\beta_1 = \mu_{t-t'}^0$, the decomposition (32) of β can now be resolved to read

$$\beta = \left(\theta_2 - q_{00} \frac{1 - \theta_2}{1 - q_{00}} \right) \mu_{t-t'}^0 + \frac{1 - \theta_2}{1 - q_{00}} \mu_{t-t'+1}^0, \quad (33)$$

which completes expression (30) and proves (26b) for the off-diagonal elements of the covariance matrix. \square

Remark 9: The expectation and covariance in equations (14) and (26) depend on the eigenvalues and eigenvectors of the matrix $M = M^s M^\ell$, but not on the single transition probabilities in M^s and M^ℓ directly. From joint knowledge of μ and Σ , the parameters $v_0, q_{00}, \alpha_x^0, \alpha_x^1, \lambda_x, \theta_1, \theta_2$, and θ_3 are identifiable. Not all of them, however, are independent (see Lemma 3), and knowing these parameters is in general not sufficient to reconstruct the matrices M^s and M^ℓ . Plots of μ and Σ as well as simulation results for the processes X and Y are depicted in Figure 5 and 6.

Remark 10 (variance “dip”): Figure 5d illustrates a characteristic property of the variance Σ_{tt} in dependence of the frame number t . Initially, the variance increases for some frames before it subsequently relaxes towards the background noise exponentially. This salient “dip” in the variance curve is also observed in experimental data [19] for large values of v_0 , i.e., if most fluorophores are bright at the beginning of the experiment. It is caused by bright fluorophores getting dark during the first few frames, such that the observable distribution of photons Y_t is effectively an additive model composed of two parts: dark fluorophores with Y_t close to 0 and bright ones with Y_t around θ_1 . This split in the distribution of Y_t temporarily causes a high variance until the number of dark fluorophores dominates on the long run.

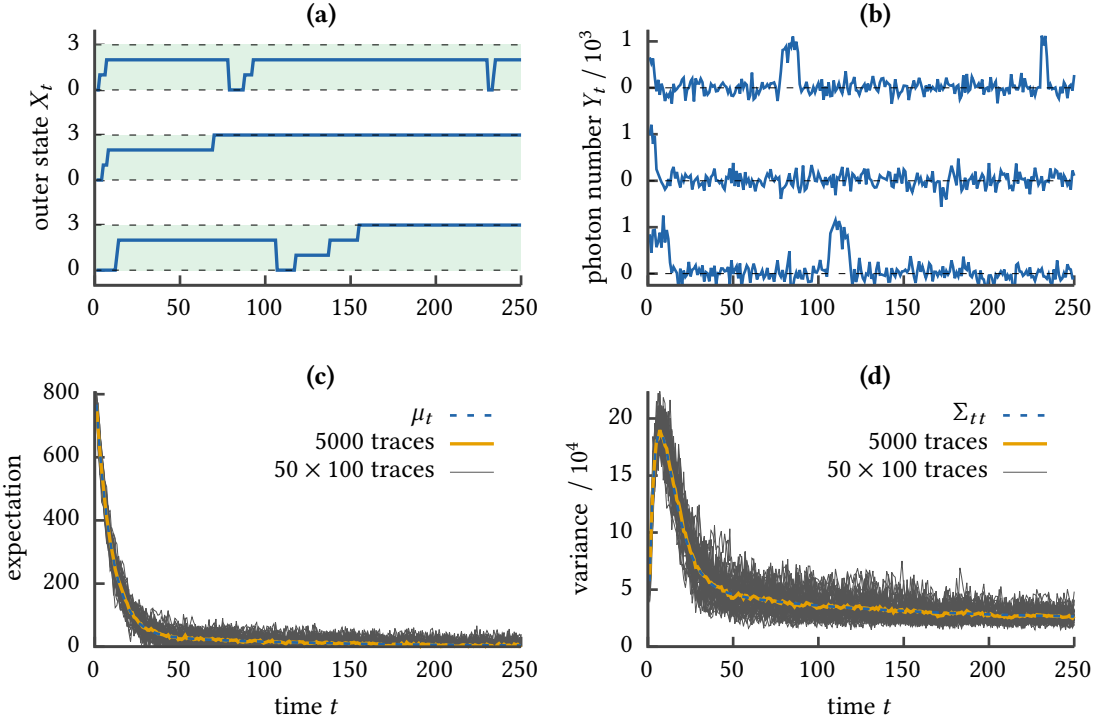


Figure 5: Simulation results of the single-fluorophore HTTM. **(a)** shows three exemplary paths of the fluorophore in the outer state space $\mathcal{S} = \{0, \dots, r\}$ for $r = 3$. One can see that two of the three fluorophores have already bleached in the first 250 time steps. **(b)** shows three fluorescence traces $y = (y_t)_{t=1}^{250}$ corresponding to the paths in **(a)**. To obtain more realistic traces, Gaussian white noise with mean 0 and standard deviation $\theta_1/5$ was added to each observation y_t . **(c-d)** show the theoretical expectation μ_t and variance Σ_{tt} of Y_t compared to their empirical estimates for 5000 and 100 simulated traces. In all simulations, we use the inner model described in Section 6. The parameters for the inner and outer model are chosen such that the resulting traces roughly resemble the experimental data in [19].

Multiple fluorophores. The signal we observe in experiments is based on the fluorescent activity of an unknown number m of fluorophores. As we will typically not be able to distinguish between the contributions resulting from different fluorophores, we can only rely on the total number $Y_t^{(m)}$ of photons emitted in frame t . It is given by the sum of m single-fluorophore processes Y^k modeled via \mathcal{F}^s ,

$$Y_t^{(m)} = \sum_{k=1}^m Y_t^k. \quad (34)$$

We make the assumption that the contributions Y^k are independent and identically distributed (see Remark 4). Even though these assumptions are approximations – conditions like the biochemical properties of the fluorophore’s neighbourhood or its spatial orientation may have a certain impact – they appear to lead to a decent description for the multi-fluorophore dynamics in practical situations [19]. The set of all multi-fluorophore models that obey the i.i.d. assumptions is henceforth denoted by \mathcal{F} .

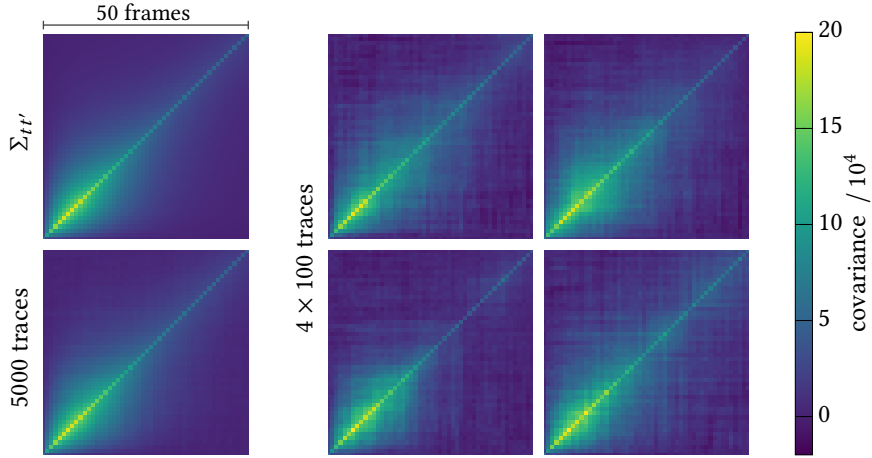


Figure 6: Real and empirical covariance of the HTTM. Shown are the covariances $\Sigma_{tt'}$ for $t, t' = 1, \dots, 50$ (upper left image) as well as their empirical counterparts for 5000 traces (lower left image) and 100 traces (four images on the right). The same simulated traces as in Figure 5c-d are used.

The expectation and covariance of $Y^{(m)}$ as sum of m i.i.d. random processes simply acquire the prefactor m with respect to the single-fluorophore expressions. Note that we will use the same symbols μ , μ^0 , and Σ as for the single-fluorophore process, see (14), (20), and (26), to denote the respective generalizations to $m \geq 1$ fluorophores.

Theorem 3: The expectation μ and covariance Σ of a multi-fluorophore process $Y^{(m)}$ in \mathcal{F} are

$$\mu_t = m \theta_1 \sum_{x \in \mathcal{S}} \alpha_x \lambda_x^{t-1} = m \theta_1 \sum_{x=0}^{r-1} (\nu_0 \alpha_x^0 + (1 - \nu_0) \alpha_x^1) \lambda_x^{t-1}, \quad (35a)$$

and

$$\Sigma_{tt} = \frac{1}{m} (m \theta_1 (\theta_3 + 1) + m - \mu_t) \mu_t, \quad (35b)$$

$$\Sigma_{tt'} = \frac{1}{m} \left[\left(\theta_2 - q_{00} \frac{1 - \theta_2}{1 - q_{00}} \right) \mu_{t-t'}^0 + \frac{1 - \theta_2}{1 - q_{00}} \mu_{t-t'+1}^0 - \mu_t \right] \mu_{t'}, \quad (35c)$$

where

$$\mu_t^0 = m \theta_1 \sum_{x \in \mathcal{S}} \alpha_x^0 \lambda_x^{t-1}, \quad (35d)$$

for $t, t' = 1, \dots, T$ with $t > t'$. The coefficients α_x , α_x^0 , and α_x^1 are given by equations (15), (21), and (22), respectively.

Parameterization. At this point, it is instructive to think about the parameterization of the multi-fluorophore model class \mathcal{F} (see also Table 1 on page 26). The full model for the photon emission process $Y_t^{(m)}$ depends on the fluorophore number m , on all transition probabilities $Q = (q_{xz})$, on the initial state v , and on an unspecified number of parameters that come with a concrete choice of the inner model. If we only want to describe the first two moments μ and Σ , however, several parameters become hidden and are not required to be estimated for our purposes.

According to equations (35a-d), we only need the fluorophore number m , the fraction of initially bright fluorophores v_0 , the probability q_{00} for a fluorophore to stay bright during the exposure, and the eigenvalues $\lambda = (\lambda_x)_{x \in S}$ as well as coefficients $\alpha^0 = (\alpha_x^0)_{x \in S}$ and $\alpha^1 = (\alpha_x^1)_{x \in S}$ for the multi-exponential decay in order to calculate the expectation and covariance. The parameters m and v_0 contribute one degree of freedom each, while q_{00} is fixed by λ and α^0 due to equation (25a). To specify λ , assuming it is real, we need r free components since $\lambda_r = 1$ is determined through the bleached state. Similarly, $\alpha_r^0 = \alpha_r^1 = 0$. Due to the constraints (25) in Lemma 3, the parameters α^0 and α^1 hence contribute $r - 1$ free components each. This makes a total number of $3r$ independent parameters, compared to $r^2 + (r - 1)$ degrees of freedom needed to specify all components of Q and v .

The three parameters $\theta = (\theta_1, \theta_2, \theta_3)$ are sufficient to specify the effect of the inner model in the second-order description. Still, specific knowledge of the inner model is necessary, since the relation of θ to other parameters is unclear otherwise. For example, an inner model with a Poissonian photon statistics $Y_t | X'_t = 0$ enforces $\theta_3 = 0$, which evidently reduces the number of free parameters. Similarly, θ_2 is not a free parameter for the inner model that we employ to describe the fluorophore Alexa 647 in Section 6; it is completely determined by q_{00} .

A setting we want to emphasize is the one where $v_0 = 1$, i.e., where each fluorophore is bright at the beginning of the experiment. This can be enforced by the experimental setup, like in the super-resolution scheme applied in [19]. Then, the $r - 1$ parameters that are needed to specify the coefficients α^1 drop out of the formulae for μ and Σ , which makes this choice particularly beneficial.

4 Image Acquisition

In the previous section, we introduced an elaborate statistical model \mathcal{F} for the number of photons that are generated by a set of m fluorophores during a series of exposures in super-resolution microscopy. We next look at the image acquisition procedure and discuss the relation between the photon emission process $Y^{(m)}$ and the final time trace $\tilde{Y}^{(m)}$ captured by the CCD camera. Fortunately, most processing steps subsequent to the emission of photons – like thinning in the microscope or amplification through the CCD camera – can be included into the model by modifying the photon statistics p_{00} and p_{10} , see (8). Consequently, merely the parameters $\theta = (\theta_1, \theta_2, \theta_3)$ will be affected in our second-order description, and equations (35a–35d) for the expectation μ and the covariance Σ will remain intact: we just need to substitute θ by suitable

transformed parameters θ' .¹

It might thus seem superfluous to explicitly model any further steps in the microscope and camera, since we will typically estimate θ from the data anyway. However, there are several reasons why it is important to understand how the original parameter θ is transformed to θ' . First, these transformations could alter the constraints placed on parameters by the inner model (like $\theta_3 = 0$ if $Y_t | X'_t = 0$ is Poissonian) by possibly introducing new parameters (such that θ'_3 could be a free parameter again, e.g., due to an unknown variance of the amplification for the specific camera model). Second, the relation between θ and θ' could be interesting in its own right, because θ contains immediate information about the actual physics of the fluorophore, while θ' merges this information with further details of the experimental setup. This additional degree of insight could also be helpful for Bayesian inference approaches, where prior knowledge about the parameters is taken into account.

Thinning. In Section 2, we mentioned that only a certain fraction of emitted photons hit the detector interface and are registered at some CCD pixel. Many photons will fail to reach the optical pathway or will be absorbed by the equipment (like lenses or mirrors). The probability that an emitted photon triggers a photo electron in a specified region of interest R of the camera was denoted by p_d , such that

$$Y'_t \sim \text{Bin}(Y_t, p_d) \quad (36)$$

models the thinned photon number for a single fluorophore. The parameter transformation from θ to θ' that accompanies this thinning process can be established by plugging Y'_t in equations (12a–c) defining the inner parameters.

Lemma 4: The moment parameters θ' of the thinned photon statistics (36) are given by

$$\theta'_1 = p_d \theta_1, \quad \theta'_2 = \theta_2, \quad \theta'_3 = \theta_3. \quad (37)$$

Therefore, only θ_1 is affected by binomial thinning while θ_2 and θ_3 are left unaffected.

Proof. Employing definitions (12a–c) yields

$$\begin{aligned} \theta'_1 &= \mathbb{E}[Y'_t | X'_t = 0] = \mathbb{E}[\mathbb{E}[Y'_t | Y_t] | X'_t = 0] \\ &= p_d \mathbb{E}[Y_t | X'_t = 0] = p_d \theta_1, \end{aligned}$$

¹ This is not entirely accurate. Camera noise contributions that do not depend on the fluorophore and its state of activity, which we called ϵ_t in equation (1) of Section 2, cannot be modeled that way and have to be considered separately. Their inclusion in the inner model would require a signal $Y_t > 0$ even for fluorophores in dark states $X'_t > 0$, which we explicitly prohibited during our derivations of μ and Σ in the previous section.

as well as

$$\begin{aligned}\theta'_2 &= q_{00} \frac{\mathbb{E}[Y'_t | X' = X = 0]}{\theta'_1} \\ &= q_{00} \frac{p_d \mathbb{E}[Y_t | X' = X = 0]}{p_d \theta_1} = \theta_2,\end{aligned}$$

and, if we use the law of total variance,

$$\begin{aligned}\theta'_3 &= \frac{\text{Var}[Y'_t | X'_t = 0]}{(\theta'_1)^2} - \frac{1}{\theta'_1} \\ &= \frac{\mathbb{E}[\text{Var}[Y'_t | Y_t] | X'_t = 0] + \text{Var}[\mathbb{E}[Y'_t | Y_t] | X'_t = 0]}{(\theta'_1)^2} - \frac{1}{\theta'_1} \\ &= \frac{p_d(1 - p_d)\theta_1 + p_d^2 \text{Var}[Y_t | X'_t = 0]}{p_d^2 \theta_1^2} - \frac{1}{p_d \theta_1} \\ &= \frac{\text{Var}[Y_t | X'_t = 0]}{\theta_1^2} - \frac{1}{\theta_1} = \theta_3.\end{aligned}$$

□

Signal amplification. When photo electrons are read out in an EMCCD camera, an electron amplifying system that consists of a cascade of electron multipliers (EM) is triggered. Each stage of this cascade has a certain probability of generating extra electrons, and the succession of many stages results in a stochastic signal amplification of the incident photons. This introduces additional noise, which we consider in the following.

We denote the distribution that results from the signal amplification of a single photo electron by \mathcal{D} , like in Section 2. For convenience, we use the symbol Y' to denote a random variable with the stationary distribution of $Y'_t | X'_t = 0$, i.e., we condition our considerations on bright fluorophores. Then, the number E of electrons generated by Y' detected photons is

$$E = \sum_{k=1}^{Y'} U_k,$$

where $U_k \sim \mathcal{D}$. By the law of total variation we obtain

$$\frac{\text{Var}[E]}{\mathbb{E}[E]^2} = \frac{\text{Var}[U_1]}{\mathbb{E}[U_1]^2} \frac{1}{\mathbb{E}[Y']} + \frac{\text{Var}[Y']}{\mathbb{E}[Y']^2}. \quad (38)$$

If Y' was Poisson distributed with parameter $\lambda > 0$, it would follow that

$$\frac{\text{Var}[E]}{\mathbb{E}[E]^2} = \left(\frac{\text{Var}[U_1]}{\mathbb{E}[U_1]^2} + 1 \right) \frac{1}{\lambda}.$$

For this reason, the term

$$f^2 = \frac{\text{Var}[U_1]}{\mathbb{E}[U_1]^2} + 1 \quad (39)$$

is called the “excess noise factor”. For the amplification models considered in [25, 17], we have $1 \leq f^2 \leq 2$. The factor f^2 is usually known for a given camera.

For each frame, the camera accumulates the photo electrons over a certain length of time, the exposure time, before multiplying them. Afterwards, the accumulated and multiplied electrons E pass through the A/D converter, which introduces a factor $c > 0$ between the actual mean number of amplified electrons and the output signal. The (ideal) output signal \tilde{Y} produced by a bright fluorophore is thus given by

$$\tilde{Y} = cE. \quad (40)$$

Similar to the case of thinning, this transformation of the photon statistics corresponds to a transformation of the inner parameters of the model from θ to θ' . This time, we find the transformation rules

$$\theta'_1 = a\theta_1, \quad \theta'_2 = \theta_2, \quad \theta'_3 = \theta_3 + \frac{f^2 - 1}{\theta_1}, \quad (41)$$

where

$$a = c \frac{\mathbb{E}[E]}{\mathbb{E}[Y']} \quad (42)$$

is the overall amplification factor that translates from detected photons Y' to the CCD output \tilde{Y} . Result (41) follows from utilizing relation (38) in expression (12c).

Offset and background. Equation (40) is an idealization of the true camera output. It neglects background photons in the setup as well as additional noise from the analog circuits and the A/D converter. Furthermore, a positive offset is usually applied to the pixel values in order to avoid noise induced fluctuations into the negative domain. In contrast to our previous considerations, all of these effects cannot be integrated into the parameters θ because they do not exclusively affect the photon statistics p_{00} and p_{10} . Instead, they are independent of the state X'_t of the fluorophore. The true multi-fluorophore output signal observed in the region R in frame t is given by

$$\tilde{Y}_t^{(m)} = cE_t + o + \epsilon_t, \quad (43)$$

where E_t is the respective amplified number of electrons in frame t , o is an offset value, and ϵ_t is a centered random variable that subsumes all additional noise sources and is considered to be independent of E_t . Usually, the standard deviation σ_t of ϵ_t will be small compared to the total image background noise. It may depend on time, since the camera electronics may adapt during the experiment. Together with the offset o , σ_t can be estimated from the image series directly.

We want to remark that the parameter a in (42) can also be estimated directly [17]. This can be done by illuminating the camera with a temporally constant but spatially inhomogeneous light intensity, which leads to Poisson statistics in each pixel with an inhomogeneous parameter. One can then estimate the mean and variance of the camera outputs \tilde{Y} at each pixel from a

time series of such images, and determine af^2 as the slope in a plot of $\text{Var}[\tilde{Y}]$ against $\mathbb{E}[\tilde{Y}]$ with known f^2 , since

$$\text{Var}[\tilde{Y}] = c^2 \text{Var}[E] + \text{Var}[\epsilon] = c^2 f^2 \frac{\mathbb{E}[E]^2}{\mathbb{E}[Y']} + \text{Var}[\epsilon] = af^2 \mathbb{E}[\tilde{Y}] + \text{const.}$$

Remarks and full model. The preceding considerations show how the modeling steps of thinning and signal amplification transform the inner model parameters θ . Other contributions, like background photons, cannot be included in the description by merely modifying θ . Some of the emerging parameters are known (like the excess noise f^2) or can be estimated independently from the fluorophore model (like the amplification factor a , the offset o , and the variance σ_t^2 of the background noise ϵ_t). The detection probability p_d , however, cannot be separated from the expected number of photons θ_1 during inference, which is why we will drop p_d from the final model formulation, effectively working with $\theta' = p_d \theta$. We also assume preprocessed image data, where the offset o has been subtracted and where the signal was divided by the total amplification a , i.e., we actually consider normalized data that is modeled by

$$\frac{\tilde{Y}_t^{(m)} - o}{a}. \quad (44)$$

Our full second order description for fluorescence time traces is thus captured by the following theorem, the notation of which is summarized by Table 1 on page 26.

Theorem 4: The mean μ and the covariance Σ of the normalized process (44), which models the fluorophore activity observed by a camera, are given by

$$\mu_t = m \theta_1 \sum_{x=0}^{r-1} (\nu_0 \alpha_x^0 + (1 - \nu_0) \alpha_x^1) \lambda_x^{t-1}, \quad (45a)$$

$$\Sigma_{tt} = \frac{1}{m} (m \theta_1 (\theta_3 + 1) + mf^2 - \mu_t) \mu_t + \sigma_t^2 / a^2, \quad (45b)$$

$$\Sigma_{tt'} = \frac{1}{m} \left[\left(\theta_2 - q_{00} \frac{1 - \theta_2}{1 - q_{00}} \right) \mu_{t-t'}^0 + \frac{1 - \theta_2}{1 - q_{00}} \mu_{t-t'+1}^0 - \mu_t \right] \mu_{t'}, \quad (45c)$$

where

$$\mu_t^0 = m \theta_1 \sum_{x=0}^{r-1} \alpha_x^0 \lambda_x^{t-1}, \quad (45d)$$

for $t, t' = 1, \dots, T$ with $t > t'$.

Proof. The respective expressions follow from combining equations (35a-d) for the multi-fluorophore model $\tilde{Y}_t^{(m)}$ together with result (41) and definition (43) established in this section. \square

Symbol	Meaning	Reference	Comment
<i>stochastic fluorophore dynamics</i>			
X_t	state after t -th exposure	p. 9	
X'_t	state before t -th exposure	p. 9	
Y_t	photons emitted in t -th exposure	p. 9	
\tilde{Y}_t	camera output values in frame t	eq. (43), p. 24	
<i>general model specification</i>			
M^ℓ, M^s	long/short-time transition matrix	eq. (3a), p. 9	constrained in eq. (6)
$v = (v_x)$	dist. of the initial state X_0	p. 9	
q_{xz}	constrained transition probabilities	eq. (6), p. 11	entries of M^ℓ and M^s
p_{xz}	photon statistics	eq. (4), p. 9	dist. of $Y_t X_t = x, X'_t = z$, constrained in eq. (8)
(*) m	number of i.i.d. fluorophores	p. 19	central quantity of interest
<i>second order specification</i>			
(*) $\theta_1, \theta_2, \theta_3$	inner model parameters	eq. (12), p. 13	describe first two moments of $Y_t X_t = 0$, can be constrained (e.g., for Alexa 647)
(*) v_0	fraction of bright molecules at $t = 0$	p. 9	α^1 drops out if $v_0 = 1$
(*) q_{00}	prob. to stay bright in one exposure	eq. (6), p. 11	usually connected to inner parameters θ
(*) $\lambda = (\lambda_x)$	eigenvalues of $M = M^s M^\ell$	p. 13	$\lambda_x \in [0, 1]$ under suitable conditions, see appendix C
(*) $\alpha = (\alpha_x)$,	multi-exponential sum coefficients	eq. (15), p. 13	
(*) $\alpha^0 = (\alpha_x^0)$,		eq. (21), p. 15	
(*) $\alpha^1 = (\alpha_x^1)$		eq. (22), p. 15	
<i>camera and background</i>			
f^2	excess relative variance of camera	eq. (39), p. 23	
σ_t^2	background noise in frame t	p. 24	variance of ϵ_t in eq. (43)
a	overall amplification factor	eq. (42), p. 24	

Table 1: Overview of the notation and symbols used to describe the HTTM. An asterisk (*) indicates that the corresponding parameter is usually unknown and needs to be estimated (jointly) from the time traces by the methods described in section 5. The three parameters describing the influence of camera and noise can be obtained (or estimated) independently. The references refer to the first mention of the respective quantity in sections 3 and 4.

5 Estimation

In the previous sections, we have developed a statistical model for the time series of the observable fluorescence generated by m fluorophores. We now address the central goal of this article: estimating m with our model. To this end, let

$$y = (y_t)_{t=1}^T \quad (46)$$

be a realization of the process $\tilde{Y}^{(m)}$ in (43) that models the observable fluorescence during the measurement process. Practically, y is obtained from a series of microscopy images (frames) by summing the camera output values over some fixed region of interest (see [19] for details on necessary or beneficial preprocessing steps).

The fluorophore number m will not be the only unknown parameter of $\tilde{Y}^{(m)}$. Indeed, several (or even all) of the parameters $\gamma = (m, q_{00}, v_0, \alpha^0, \alpha^1, \lambda, \theta)$ that describe the first two moments of $\tilde{Y}^{(m)}$ (see Table 1) are usually not known precisely, since the properties of the fluorophore heavily depend on the fluorophore type itself and on details of the experimental setting. The preferable choice is therefore to jointly estimate all values in γ , respecting the constraints that are inherent to the model.²

Pseudo log-likelihood. The process $\tilde{Y}^{(m)}$ has a complicated non-Gaussian and non-stationary structure with long term correlations. Furthermore, it is essentially impossible to evaluate the likelihood function numerically for a given set of parameters, since it consists of too many terms (see Remark 5). This makes direct likelihood-based methods to estimate the model parameters γ unsuitable. To overcome this difficulty, we approximate $\tilde{Y}^{(m)}$ by a Gaussian process with known parametric form of the expectation $\mu = \mu(\gamma)$ and covariance $\Sigma = \Sigma(\gamma)$ (see equations (45a-d)). This leads to the *pseudo log-likelihood*

$$\tilde{l}_y(\gamma) = -\frac{1}{2} \left[(y - \mu) \Sigma^{-1} (y - \mu) + \log \det \Sigma \right], \quad (47)$$

where we neglect an additive constant that would belong to the full log-likelihood of the Gaussian process. We estimate the model parameters γ by finding a set of values $\hat{\gamma}$ that maximize this expression,

$$\hat{\gamma} = \arg \max_{\gamma \in \Gamma} \tilde{l}_y(\gamma). \quad (48)$$

While this approach significantly simplifies the estimation compared to direct treatment of $\tilde{Y}^{(m)}$, equation (48) still represents a non-convex optimization problem over a parameter space Γ that obeys several (non-linear) constraints. As such, there is neither a closed theory nor a canonical method for numerical treatment available.

In the general case, where all parameters in γ need to be estimated and no additional constraints can be posed, Γ will be a manifold of dimension $3r + 3$ (see the discussion at the end of Section

² See the end of Section 3 for a general discussion of these constraints, and Section 6 for a discussion in context of the fluorophore Alexa 647.

3). For specific choices of the inner model, there could be fewer free parameters in θ , reducing the dimension of Γ . If v_0 is known and not equal to 1 or 0, there is 1 parameter less. If it is known and equal to 1 or 0, then there are even r free parameters less, because α^1 respectively α^0 drop out of the expressions in (45). In case of Alexa 647, with a model of $r = 3$ dark states and an additional constraint on θ_2 , see Section 6, we are thus confronted with an 8, 10, or 11-dimensional parameter space Γ .

Numerical procedure. Finding a numerical solution of the optimization problem (48) poses several challenges. First, the high dimensionality of Γ in combination with both equality and inequality constraints forces one to apply very general optimization schemes (like (quasi) Newton methods, primal-dual-splitting, or nonlinear conjugate gradient methods). Some of these schemes rely on gradient information about $\tilde{l}_y(\gamma)$ while others are gradient-free. All of them, however, work in a local fashion and thus crucially rely on the choice of suitable initial parameters γ_{init} . Indeed, optimizing over all parameters of γ simultaneously was empirically found to depend sensitively on the initial values and did not always converge to the global maximum in reasonable time. Instead, approaches where different components of γ were held fixed at times – and partial optimizations were conducted sequentially – turned out to be most successful.

To find suitable initial parameters, different methods can be applied. One option is to first employ a multi exponential fit of the expectation value μ_t . This will yield first guesses for λ and for the product $m\theta_1\alpha$. However, this fit may be of poor quality if the number r of dark states is large. The value of θ_1 may furthermore be guessed from late segments in the time traces, where with high probability at most one fluorophore is active due to bleaching. In case of the experimental data analyzed in [19], we eventually found a set of initial parameters that worked well on a range of different image series in experimentally similar conditions.

6 Case Study: Alexa 647

In the following, we specialize our general model for the fluorophore Alexa 647, which was used in the experimental work of [19]. Fluorophores of the Alexa series are popular in diverse areas of biomedical research. Due to their properties, like high photostability and brightness, they are amongst the most common choices for super resolution microscopy markers for in vitro cell experiments. Alexa 647 dyes can be used to label a wide variety of molecules, e.g., DNA [19] or proteins like IgG antibodies, streptavidin, or transferrin [4]. They have their absorption maximum at 650 nm and their emission maximum at 671 nm.

Markov model. We focus on the inner and outer models that are illustrated in Figure 3. According to the statistical fluorophore model \mathcal{F}^s established in Section 3, we need several components in order to describe the full fluorophore behavior: the inner and outer transition matrices M^s and M^l , represented by the values $Q = (q_{xz})$, and the photon statistics $p_{00}(y)$ and

$p_{10}(y)$. The outer model depicted in Figure 3 has $r = 3$ dark states, and the respective transition matrix is given by

$$M^\ell = \begin{pmatrix} 1 & q_{01} & q_{02} & 0 \\ 0 & q_{11} & q_{12} & 0 \\ 0 & q_{21} & q_{22} & 0 \\ 0 & q_{31} & q_{32} & 1 \end{pmatrix}.$$

The inner model, in contrast, is given through a Markov chain with inner states S_0 , S_1 , and D_3 . We furthermore include an “exit” state E (see Remark 7) in our description, which indicates the transition to one of the dark states of the outer model. This is the only possibility for the fluorophore to leave the bright state during exposure. The short-time matrix M^s for $r = 3$ is

$$M^s = \begin{pmatrix} q_{00} & 0 & 0 & 0 \\ q_{10} & 1 & 0 & 0 \\ q_{20} & 0 & 1 & 0 \\ q_{30} & 0 & 0 & 1 \end{pmatrix}.$$

Photons are emitted in this inner model if the fluorophore makes the transition from the excited singlet state S_1 to the ground state S_0 .

Note that this model for Alexa 647 is not an exact representation of the quantum mechanical state diagram of the fluorophore, which would require the inclusion of a high number of states that each possess vibrational and rotational substates. However, the full details of the quantum mechanical energy landscape are unknown for most fluorophores, and, according to Remark 1, they also do not have to be known, since states that live on similar time scales can be identified. In fact, it appears from the empirical study in [19] that the description provided above captures the essential features of the observed behavior of Alexa 647. Furthermore, this Markov model – or slight modifications thereof – should be appropriate to model other fluorophores, too.

Photon statistics. We now derive the photon statistics p_{00} and p_{10} for a single exposure. Our derivation is not based on a rigorous treatment of the inner Markov chain in Figure 3 but on a reasonable approximation. For convenience, we will use the symbol Y to refer to a random variable that has distribution $Y_t | X'_t = 0$ in the following. This means that Y will *not* refer to the single fluorophore process $(Y_t)_{t=1}^T$ for the duration of this section.

Let us call a maximal uninterrupted sequence of transitions between S_0 and S_1 a “burst”. A burst is ended by a transition to D_3 . This leads to a geometric distribution: do the loop $S_0 \rightarrow S_1 \rightarrow S_0$ until failure $S_1 \rightarrow D_3$. Calling the probability of failure $p \in (0, 1)$, it is clear that the number of loops, and hence the number of photons in this burst, has a geometric distribution with parameter $1 - p$. During each exposure interval, there will be a number of B bursts such that the total number of photons Y is a sum of B independent geometrically distributed random variables. This leads to a negative binomial distribution with parameters B and $1 - p$,

$$Y \sim \text{NegBin}(B, 1 - p).$$

The number of bursts B is a random quantity. To determine its distribution, first consider the case that occurs when the bright state can never be left. Then the distribution of B would be approximately Poissonian: dividing the exposure interval into many small intervals, each much longer than a typical burst but much smaller than the exposure time³, there is a small probability for a burst in each interval and a large number of intervals such that one is in the Poisson limit of the binomial distribution. When taking into account the transition to the exit state E , there is a nonzero probability for a “failure” (i.e., exiting) before each burst. Hence, every burst can be viewed as one successful trial, and the bursts continue until either the exit state or the end of the exposure time is reached. Therefore, the number of bursts is given by the minimum of a Poissonian and a geometric random variable that are independent of each other,

$$\begin{aligned} B &= \min(Z, G), \\ Z &\sim \text{Poisson}(\mu), \\ G &\sim \text{Geom}(1 - q), \end{aligned}$$

with parameters $\mu > 0$ and $0 < q < 1$. The transition to the exit state happens if and only if a failure happened before the end of the exposure time. This is the case when $Z > G$. The following result provides a connection between the parameters q and μ of the photon distribution and the parameter q_{00} of the transition matrix M^s .

Lemma 5: The Alexa 647 fluorophore stays in the bright state during exposure with probability

$$q_{00} = \mathbb{P}(Z \leq G) = e^{-(1-q)\mu}. \quad (49)$$

Proof. Direct calculation yields

$$\begin{aligned} \mathbb{P}(Z > G) &= \sum_{z=0}^{\infty} \mathbb{P}(Z = z) \mathbb{P}(G < z) = \sum_{z=0}^{\infty} e^{-\mu} \frac{\mu^z}{z!} \sum_{k=0}^{z-1} q^k (1-q) \\ &= \sum_{z=0}^{\infty} e^{-\mu} \frac{\mu^z}{z!} (1 - q^z) = 1 - \sum_{z=0}^{\infty} e^{-\mu} \frac{(q\mu)^z}{z!} \\ &= 1 - e^{-(1-q)\mu} = 1 - q_{00}, \end{aligned}$$

which shows the claim. \square

We next derive the moment generating function G of Y . It can be expressed via the moment generating function G^B of the number B of bursts.

³ This is possible due to the large difference in transition rates between $S_0 \rightarrow S_1$ and $D_3 \rightarrow S_0$.

Lemma 6: The moment generating function of Y is given by

$$G(\xi) = G^B \left(\log \left(\frac{1-p}{1-pe^\xi} \right) \right), \quad (50)$$

where

$$\begin{aligned} G^B(\xi) &= e^{-(1-q)\mu} e^{-(1-e^\xi)q\mu} + (1 - e^{(1-q)\mu}) \frac{1-q}{1-qe^\xi} \frac{1 - e^{-(1-qe^\xi)\mu}}{1 - e^{(1-q)\mu}} \\ &= q_{00} G_{00}^B(\xi) + (1 - q_{00}) G_{10}^B(\xi). \end{aligned} \quad (51)$$

The functions G_{00}^B and G_{10}^B denote the generating functions of B conditioned on $Z \leq G$ and $Z > G$, respectively.

Proof. Calculation shows

$$\begin{aligned} G^B(\xi) &= \mathbb{E}[e^{\xi B}] = \mathbb{E}\left[\mathbb{E}[e^{\xi B} | Z]\right] \\ &= \mathbb{E}\left[\sum_{k=0}^{Z-1} e^{\xi k} q^k (1-q) + \sum_{k=Z}^{\infty} e^{\xi Z} q^k (1-q)\right] \\ &= \mathbb{E}\left[(1-q) \frac{1 - (qe^\xi)^Z}{1 - qe^\xi} + (qe^\xi)^Z\right] \\ &= (1 - e^{(1-q)\mu}) \frac{1-q}{1-qe^\xi} \frac{1 - e^{-(1-qe^\xi)\mu}}{1 - e^{(1-q)\mu}} + e^{-(1-q)\mu} e^{-(1-e^\xi)q\mu}. \end{aligned}$$

The decomposition of G^B that is implied in (51) states that B given the event $Z \leq G$ is Poisson distributed with the reduced parameter μq . This can be established as follows:

$$\mathbb{P}(Z = z | Z \leq G) = \frac{\mathbb{P}(Z = z) \mathbb{P}(z \leq G)}{\mathbb{P}(Z \leq G)} = \frac{\frac{\mu^z}{z!} e^{-\mu} \sum_{k=z}^{\infty} q^k (1-q)}{e^{-(1-q)\mu}} = \frac{(\mu q)^z}{z!} e^{\mu q}. \quad (52)$$

Finally, we have

$$G(\xi) = \mathbb{E}[e^{\xi Y}] = \mathbb{E}\left[\mathbb{E}[e^{\xi Y} | B]\right] = \mathbb{E}\left[\left(\frac{1-p}{1-pe^\xi}\right)^B\right] = G^B \left(\log \left(\frac{1-p}{1-pe^\xi} \right) \right)$$

for the moment generating function of Y . \square

Similar results hold for the conditional generating functions G_{00} and G_{10} , which are expressible by G_{00}^B and G_{10}^B in a likewise fashion. Therefore, the photon statistics p_{00} and p_{10} are completely specified in terms of the inner parameters p , q , and μ by equations (50) and (51).

Moments. In order to understand the effects of our inner model for the second-order description of the fluorophore, we look at the parameters θ_1 , θ_2 , and θ_3 as introduced in (12).

Lemma 7: In the Alexa 647 inner model, we have the following moment parameters:

$$\theta_1 = \frac{p}{1-p} \frac{q}{1-q} (1 - q_{00}), \quad (53a)$$

$$\theta_2 = -\frac{q_{00} \log q_{00}}{1 - q_{00}}, \quad (53b)$$

$$\theta_3 = \frac{2}{1 - q_{00}} \left(\frac{1 - q}{q} - \theta_2 + 1 \right) - 1. \quad (53c)$$

Proof. All parameters can be expressed via derivatives of the generating functions G and G_{00} at zero. We find

$$\theta_1 = \mathbb{E}[Y] = G'(0) = \frac{p}{1-p} \frac{q}{1-q} (1 - q_{00})$$

for the unconditioned expectation. Similarly, one can calculate

$$\theta_2 = \frac{q_{00} \mathbb{E}[Y | Z \leq G]}{\theta_1} = \frac{q_{00}}{\theta_1} G'_{00}(0) = -\frac{q_{00} \log q_{00}}{1 - q_{00}}.$$

Finally, the parameter θ_3 can be computed to read

$$\theta_3 = \frac{\text{Var } Y}{\theta_1^2} - \frac{1}{\theta_1} = \frac{G''(0)}{\theta_1^2} - \frac{1}{\theta_1} - 1 = \frac{2}{1 - q_{00}} \left(\frac{1 - q}{q} - \theta_2 + 1 \right) - 1,$$

which captures the variance of Y relative to θ_1 . \square

Surprisingly, according to equations (53b) and (49), the parameter θ_2 only depends on the internal parameters via $q_{00} = e^{-(1-q)\mu}$. For reference, we note that this relation can be inverted by the formula

$$q_{00} = -\frac{\theta_2}{W_{-1}(-\theta_2 e^{-\theta_2})},$$

where W_{-1} is the branch of the Lambert- W function whose range contains the interval $(-\infty, -1/e)$ of the real line (see, e.g., [7] for a definition and a review of some properties of this function). This consideration shows that even though the inner model in Figure 3 depends on three independent parameters (p , q , and μ), only two free parameters, namely θ_1 and θ_3 , remain in the second-order description. This must be taken into account when formulating and conducting the optimization routine for the pseudo log-likelihood (47) used to estimate the model parameters.

Invariance under thinning. There is another remarkable feature of this inner model choice that deserves to be highlighted. In Section 4, we derived how thinning – the independent loss of photons with a certain probability – affects the parameters $\theta = (\theta_1, \theta_2, \theta_3)$, and we concluded that θ_1 is transformed to $\theta'_1 = p_d \theta_1$ while θ_2 and θ_3 are left untouched. Interestingly, we can make a much stronger statement for our model of Alexa 647.

Lemma 8: The parametric family of the distribution Y for Alexa 647 is left invariant by thinning.

Proof. Let $D_1, D_2, \dots \sim \text{Ber}(p_d)$ be independently Bernoulli distributed, and let $G^D(\xi)$ be the moment generating function of D_1 ,

$$G^D(\xi) = \mathbb{E}(e^{\xi D_1}) = 1 + p_d(e^\xi - 1). \quad (54)$$

The thinned photon count is given through $Y' \sim \text{Bin}(Y, p_d)$, which can also be stated as

$$Y' = \sum_{i=1}^Y D_i.$$

The moment generating function of Y' is

$$G^{Y'}(\xi) = \mathbb{E}\left[\mathbb{E}[e^{\xi Y'} | Y]\right] = \mathbb{E}[e^{\log(G^D(\xi))Y}] = G(\log G^D(\xi)),$$

where G denotes the generating function of Y . When we define the transformed probability

$$p' = \frac{p p_d}{1 - p + p p_d}, \quad (55)$$

we can invoke expression (50) for G and equation (54) for G^D to find

$$G^{Y'}(\xi) = G^B\left(\log\left(\frac{1-p}{1-p(1+p_d(e^\xi-1))}\right)\right) = G^B\left(\log\left(\frac{1-p'}{1-p'e^\xi}\right)\right).$$

Comparison to equation (50) reveals that the distribution of detected photons has the same parametric form as without thinning, and the only effect is the monotone transformation (55) of the geometric probability p . The same statement holds for the generating functions conditioned on $Z > G$ or $Z \leq G$, so the parametric family of the photon statistics for our model of Alexa 647 is indeed left invariant by thinning. \square

A Lumped Markov Chains

Like for most biochemical compounds, the precise quantum physical state space of fluorophores is likely to be much more involved than our relatively simple four (outer) state model for Alexa 647 (see Section 6). Still, modeling fluorophores and other biochemical molecules as Markov chains with a smaller number of states than actual quantum states works often very well. In the following, we briefly outline that states with the same transition rates can be combined into single states without losing the Markov property. Our exposition follows [18].

Let \mathcal{S} denote the finite state space of a stationary Markov chain $X = (X_t)_{t \in \mathbb{N}}$ with transition Matrix M . Let $P = \{\mathcal{S}_1, \dots, \mathcal{S}_k\}$ be a partition of \mathcal{S} , and let $\pi: \mathcal{S} \rightarrow P$ be the respective

projection map, meaning $\pi(x) = \mathcal{S}_i$ iff $x \in \mathcal{S}_i$ for some $i = 1, \dots, k$. The stochastic process defined by $\pi \circ X$ is called the *lumped process*, where only states can be observed which are merged according to the partition P . Furthermore, the chain X is called *lumpable* with respect to P if $\pi \circ X$ is again a Markov chain for any initial distribution on X . Similarly, X is called *weakly lumpable* if the lumped process is Markov for some initial distribution on X .

Theorem (Kemeny and Snell, 1960): A necessary and sufficient condition for a Markov chain to be lumpable with respect to a partition P is that for every pair of sets \mathcal{S}_i and \mathcal{S}_j in P , the probabilities

$$p_{\mathcal{S}_j x} = \sum_{z \in \mathcal{S}_j} M_{zx}$$

to transition to \mathcal{S}_j from x have the same value for every $x \in \mathcal{S}_i$. These common values form the transition matrix for the lumped chain $\pi \circ X$.

Proof. The proof can be found in [18], Theorem 6.3.2. Note that Kemeny and Snell consider row-stochastic transition matrices while we use column-stochastic ones. \square

In the case of interest to us, the partition P of \mathcal{S} corresponds to groupings of physical fluorophore states that have (approximately) the same transition rates to states of other groups. It is easy to check that the conditions for the above theorem are satisfied in this setting and that the lumped chain is thus Markov.

Corollary: Let P be a partitioning $\{\mathcal{S}_1, \dots, \mathcal{S}_k\}$ of states \mathcal{S} such that for all $i = 1, \dots, k$

$$M_{zx} = M_{zx'} \quad \text{for all } x, x' \in \mathcal{S}_i \text{ and } z \in \mathcal{S} \setminus \mathcal{S}_i. \quad (56)$$

Then the Markov chain X is lumpable with respect to P .

Proof. For $i \neq j$, it immediately follows from (56) that

$$p_{\mathcal{S}_j x} = \sum_{z \in \mathcal{S}_j} M_{zx} = \sum_{z \in \mathcal{S}_j} M_{zx'} = p_{\mathcal{S}_j x'}$$

for all x, x' in \mathcal{S}_i . If $i = j$, we similarly find

$$p_{\mathcal{S}_i x} = 1 - \sum_{z \in \mathcal{S} \setminus \mathcal{S}_i} M_{zx} = 1 - \sum_{z \in \mathcal{S} \setminus \mathcal{S}_i} M_{zx'} = p_{\mathcal{S}_i x'}.$$

Therefore, $p_{\mathcal{S}_j x}$ does not depend on $x \in \mathcal{S}_i$ for all $j = 1, \dots, k$, and the theorem of Kemeny and Snell can be applied. \square

B Diagonalizability of Stochastic Matrices

Let \mathcal{M} be the set of stochastic $n \times n$ matrices with a fixed $n \geq 2$. A (column) stochastic matrix $M \in \mathcal{M}$ has only non-negative entries and its columns sum to 1. Therefore, the set \mathcal{M} forms an $n(n-1)$ -dimensional submanifold of the unit cube $[0, 1]^{n \times n}$. In the following, we want to show that it is reasonable to assume that a randomly picked matrix in \mathcal{M} is diagonalizable with probability one.

To this end, we consider the following projection map π from $[0, 1]^{n \times n}$ to \mathcal{M} . We represent values in $[0, 1]^{n \times n}$ by $v = (v_1, \dots, v_n)$, where each v_i is a column vector in $[0, 1]^n$. Let \tilde{v}_i denote the normed vector

$$\tilde{v}_i = \frac{v_i}{\sum_{j=1}^n v_{ij}}.$$

Then, for almost all $v \in [0, 1]^{n \times n}$ with respect to the Lebesgue measure λ on $[0, 1]^{n \times n}$, we can define

$$\pi(v) = (\tilde{v}_1, \dots, \tilde{v}_n) \in \mathcal{M}.$$

Note that λ is a probability measure on $[0, 1]^{n \times n}$. Since π is measurable (assuming the subspace Borel σ -field on \mathcal{M}), we obtain the induced probability measure λ^π on \mathcal{M} , where

$$\lambda^\pi(V) = \lambda(\pi^{-1}(V))$$

for any measurable $V \subset \mathcal{M}$.

Lemma 9: Let $N \subset \mathcal{M}$ be the set of stochastic matrices that are not diagonalizable. Then

$$\lambda^\pi(N) = 0,$$

i.e., any matrix in \mathcal{M} is diagonalizable with probability one.

Proof. In the following, we only consider matrices in the open domain $(0, 1)^{n \times n}$, which have strictly positive entries. This is sufficient, since the boundary $[0, 1]^{n \times n} \setminus (0, 1)^{n \times n}$ has Lebesgue measure zero. We also define the stochastic matrices $\mathcal{M}^+ = \pi((0, 1)^{n \times n})$ with strictly positive entries.

Let $\Delta : \mathbb{R}^{n \times n} \rightarrow \mathbb{R}$ be the function that maps $A \in \mathbb{R}^{n \times n}$ to the discriminant of the characteristic polynomial of A . The characteristic polynomial of A is given by

$$\lambda \mapsto \det(A - \lambda \mathbb{1}_n),$$

where $\mathbb{1}_n$ is the identity matrix in n dimensions, and the discriminant of a polynomial with roots $\lambda_1, \lambda_2, \dots, \lambda_n \in \mathbb{C}$ is proportional to

$$\prod_{i < j} (\lambda_i - \lambda_j)^2.$$

Since the coefficients of the characteristic polynomial are polynomials in the entries of A , and since the discriminant is a real polynomial of the coefficients (see, e.g., [3]), Δ itself is a real polynomial in the entries of A . It is easy to check that Δ is not constant 0 on \mathcal{M}^+ .

The map π is real-analytical on $(0, 1)^{n \times n}$, and the map Δ is real-analytical as a function restricted to (the real-analytical manifold) \mathcal{M}^+ . Consequently, the composition

$$\Delta \circ \pi : (0, 1)^{n \times n} \rightarrow \mathbb{R}$$

is a non-constant real-analytic function. Due to the properties of the discriminant, we have that

$$\Delta(M) \neq 0 \iff M \text{ has } n \text{ distinct eigenvalues},$$

where the latter property implies diagonalizability. Thus, if $N^+ \subset \mathcal{M}^+$ denotes the set of non-diagonalizable positive stochastic matrices, we find

$$\lambda^\pi(N^+) \leq \lambda^\pi(\Delta^{-1}(0) \cap \mathcal{M}^+) = \lambda((\Delta \circ \pi)^{-1}(0)) = 0.$$

The last equality follows from the fact that the set of roots of non-zero real-analytic functions on any connected open domain of \mathbb{R}^d , $d \in \mathbb{N}$, has λ^d -Lebesgue measure zero [23]. Since the difference between N and N^+ is only a null set, the statement of the lemma follows. \square

C Real and Positive Eigenvalues

In Appendix B, we showed that essentially every transition matrix M in our fluorophore model \mathcal{F}^s is diagonalizable. Here, we argue that it is even plausible to assume real positive eigenvalues, i.e., that the spectrum $\sigma(M)$ of M is contained in $[0, 1]$ if the number r of dark states is lower than or equal to 3. The corresponding matrices for $r = 1, 2, 3$ look like

$$M_1 = \begin{pmatrix} a_1 & 0 \\ a_2 & 1 \end{pmatrix}, \quad M_2 = \begin{pmatrix} a_1 & a_2 & 0 \\ a_3 & a_4 & 0 \\ a_5 & a_6 & 1 \end{pmatrix}, \quad M_3 = \begin{pmatrix} a_1 & a_2 & a_3 & 0 \\ a_4 & a_5 & a_6 & 0 \\ a_7 & a_8 & a_9 & 0 \\ a_{10} & a_{11} & a_{12} & 1 \end{pmatrix}, \quad (57)$$

where $a_i \in [0, 1]$ for all $i = 1, \dots, r(r+1)$, and where all columns sum up to one.

The case $r = 1$ is trivial: the eigenvalues are a_1 and 1. For $r = 2$ and 3, we have to make further assumptions in order to conclude $\sigma(M) \subset [0, 1]$. If $r = 2$, we need that the diagonal values of M are large enough (see Lemma 10 below), and for $r = 3$ we additionally require that the diagonal values are sufficiently distinct, as is made precise in Lemma 12. These two assumptions – large and distinct diagonal values – are natural for our setting: the former means that the outer states are usually stable over more than one frame, while the latter holds if states with similar dwell times are merged for the Markovian description of the fluorophore (see Remark 1 and Appendix A for more details).

Lemma 10: The eigenvalues of the matrix M_2 given by (57) are real with absolute value ≤ 1 . If all diagonal entries are $\geq 1/2$, they are additionally non-negative, such that

$$\sigma(M_2) \subset [0, 1].$$

Proof. Since M_2 is a stochastic matrix, the absolute value of all eigenvalues of M_2 is bounded by 1. The characteristic polynomial Q of M_2 is

$$Q(\lambda) = (1 - \lambda)[(a_1 - \lambda)(a_4 - \lambda) - a_2 a_3] = (1 - \lambda)[\lambda^2 - (a_1 + a_4)\lambda + (a_1 a_4 - a_2 a_3)].$$

Clearly, $\lambda = 1$ is an eigenvalue. In order to ensure that all other eigenvalues are also real, we investigate the discriminant Δ of the second factor above (in square brackets). It is given by

$$\Delta = (a_1 + a_4)^2 - 4(a_1 a_4 - a_2 a_3) = (a_1 - a_4)^2 + 4a_2 a_3,$$

which satisfies $\Delta > 0$, since all entries are non-negative. Consequently, all eigenvalues are real-valued. If additionally $a_1, a_4 \geq 1/2$ (and thus $a_2, a_3 \leq 1/2$), we find

$$Q(\lambda) > a_1 a_4 - a_2 a_3 \geq 0$$

for $\lambda < 0$. Therefore, all eigenvalues must be non-negative. \square

The most important application of our theory is the Alexa 647 model described in section 6. Here, $r = 3$, which leads to a transition matrix of the form M_3 . Unlike for $r = 1, 2$, these matrices do not always have real eigenvalues. The following lemma provides an analytical criterion for all eigenvalues to be real.

Lemma 11: Assume that M_3 as given in (57) is diagonalizable and that its upper left 3×3 submatrix is irreducible. Then, besides the value 1, M_3 has a second real eigenvalue $\lambda_0 \in (0, 1]$ that is larger than or equal to the diagonal entries,

$$\max\{a_1, a_5, a_9\} \leq \lambda_0.$$

The remaining two eigenvalues of M are real if and only if

$$(\bar{a}_1 + \bar{a}_5 + \bar{a}_9)^2 + 4(a_6 a_8 + a_2 a_4 + a_3 a_7 - \bar{a}_1 \bar{a}_5 - \bar{a}_1 \bar{a}_9 - \bar{a}_5 \bar{a}_9) \geq 0, \quad (58)$$

where $\bar{a}_i = a_i - \lambda_0$.

Proof. Let M' be the upper left 3×3 submatrix of M_3 . The characteristic polynomial of M_3 is given by

$$\det(M_3 - \lambda \mathbb{1}_4) = -(1 - \lambda) \cdot \det(M' - \lambda \mathbb{1}_3), \quad (59)$$

where $\mathbb{1}_3$ and $\mathbb{1}_4$ are the identity matrices in three and four dimensions, respectively. We can therefore restrict our study to the eigenvalues of M' , which is an irreducible matrix with

non-negative entries by assumption. This allows us to apply Perron-Frobenius theory [22]. In particular, M' has a real eigenvalue $0 < \lambda_0 \leq 1$, such that all other eigenvalues of M' are smaller in absolute value. Since M' is diagonalizable, this largest eigenvalue λ_0 is equal to the operator norm of M' . In particular, λ_0 is thus larger than all diagonal entries of M' ,

$$\max\{a_1, a_5, a_9\} \leq \lambda_0, \quad (60)$$

because $a_1 = e_1^T M' e_1 \leq \lambda_0$, where $e_1 = (1, 0, 0)^T$, and analog relations hold for a_5 and a_9 . We denote the characteristic polynomial of M' by Q , and we also define the shifted polynomial

$$H(\mu) = Q(\mu + \lambda_0).$$

Then $H(0) = Q(\lambda_0) = 0$, since λ_0 is an eigenvalue of M' . Setting $\bar{a}_i = a_i - \lambda_0$, Sarrus' rule for the determinant of 3×3 matrices yields

$$\begin{aligned} H(\mu) &= \det(M' - (\mu + \lambda_0) \mathbb{1}) \\ &= (\bar{a}_1 - \mu)(\bar{a}_5 - \mu)(\bar{a}_9 - \mu) + a_2 a_6 a_7 + a_3 a_4 a_8 - a_6 a_8 (\bar{a}_1 - \mu) - a_3 a_7 (\bar{a}_5 - \mu) - a_2 a_4 (\bar{a}_9 - \mu) \\ &= -\mu^3 + (\bar{a}_1 + \bar{a}_5 + \bar{a}_9)\mu^2 + (a_6 a_8 + a_2 a_4 + a_3 a_7 - \bar{a}_1 \bar{a}_5 - \bar{a}_1 \bar{a}_9 - \bar{a}_5 \bar{a}_9)\mu, \end{aligned}$$

where we harnessed in the last step that the constant part of the polynomial H vanishes due to $H(0) = 0$. The polynomial H (and thus Q) has exclusively real roots if and only if the discriminant of H is non-negative. The discriminant of a polynomial $ax^3 + bx^2 + cx + d$ of order three is given by

$$\Delta = b^2 c^2 - 4ac^3 - 4b^3 d - 27a^2 d^2 + 18abcd.$$

In our case, where $d = 0$ and $a = -1$, we find

$$\Delta/c^2 = b^2 - 4ac = (\bar{a}_1 + \bar{a}_5 + \bar{a}_9)^2 + 4(a_6 a_8 + a_2 a_4 + a_3 a_7 - \bar{a}_1 \bar{a}_5 - \bar{a}_1 \bar{a}_9 - \bar{a}_5 \bar{a}_9)$$

for the relevant part of the discriminant of H , since $c^2 > 0$ can be assumed (if $c = 0$, $\Delta = 0$ follows and all eigenvalues are real). \square

It is easy to find examples, where condition (58) is violated, and eigenvalues are complex. For instance, the matrix

$$M_3 = \begin{pmatrix} 0.8 & 0 & 0.1 & 0 \\ 0.1 & 0.8 & 0 & 0 \\ 0.1 & 0.1 & 0.8 & 0 \\ 0 & 0.1 & 0.1 & 1 \end{pmatrix}$$

has the eigenvalues $\lambda \approx 1, 0.93, 0.73 \pm 0.06i$. The upper left 3×3 block in this matrix is irreducible, but the value in condition (58) is about -0.013 . Therefore, we need another restriction for M_3 in order to establish real eigenvalues.

Fortunately, a gap condition for the diagonal of M_3 does the trick. Assume that the diagonal values a_1, a_5, a_9 of M_3 are distinct. We order these values by magnitude and denote them by $d_1 > d_2 > d_3$. Let

$$\mu_1 = \frac{\lambda_0 - d_1}{\lambda_0 - d_2}, \quad \mu_2 = \frac{\lambda_0 - d_2}{\lambda_0 - d_3}, \quad (61)$$

where $\lambda_0 \in (0, 1]$ as in Lemma 11. Due to (60), we find that $\mu_1, \mu_2 \in [0, 1]$. The condition we need for a real spectrum is

$$\mu_2^2(1 - \mu_1)^2 \geq 2\mu_2(1 + \mu_1) - 1. \quad (62)$$

Lemma 12: If condition (62) is satisfied and Lemma 11 can be applied, the eigenvalues of the matrix M_3 given by (57) are all real, with absolute values bounded by one. If all diagonal entries of M_3 are $\geq 2/3$, it additionally holds that the spectrum is non-negative,

$$\sigma(M_3) \subset [0, 1].$$

Remark 11 (gap condition): Inequality (62) really poses a gap condition on the diagonal values, and therefore on the lifetimes of the outer states of the fluorophore. If, for example, $\mu_2 \leq 1/4$, or if both μ_1 and μ_2 are smaller than $3/8$, condition (62) will hold. Values of μ_1 and μ_2 close to 1, on the other hand, violate the inequality. In this context, further note that condition (62) is sufficient for Lemma 12 even if we replace λ_0 by 1 in definition (61) of μ_1 and μ_2 . We can therefore conclude that $\sigma(M_3) \subset [0, 1]$ is guaranteed as long as the probabilities $1 - d_i$ to leave an outer state in a time step are sufficiently diverse, i.e., the respective dwell times must be on different time scales. For instance, diagonal values

$$d_1 = 0.975, \quad d_2 = 0.95, \quad d_3 = 0.8,$$

which correspond to lifetimes of about 40, 20, and 5 microscopy frames on average, yield $\mu_1 = 1/2$ and $\mu_2 = 1/4$ for $\lambda_0 = 1$. Thus, condition (62) is satisfied and any transition matrix M_3 with these diagonal values meets the gap requirement for Lemma 12.

Proof of Lemma 12. In order to show that all eigenvalues are real, we consult Lemma 11. Condition (58) is certainly satisfied if

$$(\bar{a}_1 + \bar{a}_5 + \bar{a}_9)^2 - 4(\bar{a}_1\bar{a}_5 + \bar{a}_1\bar{a}_9 + \bar{a}_5\bar{a}_9) \geq 0.$$

Using the definition of d_i as ordered diagonal values of M_3 for $i = 1, \dots, 3$, this is equivalent to

$$(1 + \mu_2 + \mu_1\mu_2)^2 - 4(\mu_2 + \mu_1\mu_2 + \mu_1\mu_2^2) \geq 0,$$

where μ_1 and μ_2 are defined as in (61). This inequality is equivalent to (62), which can be shown by straightforward computation.

It remains to be shown that all eigenvalues are non-negative if each diagonal entry of M is $\geq 2/3$. For this, assume that there would be an eigenvalue $\lambda < 0$ of M_3 . Due to the form (59) of the characteristic polynomial of M_3 , λ must also be an eigenvalue of M' , the upper left 3×3 submatrix of M_3 . Let $v \in \mathbb{R}^3$ denote a normalized eigenvector of M' to λ . Then

$$v^T M' v = \lambda < 0 \quad (63)$$

must hold. On the other hand, if we denote the non-bleached states by $\mathcal{S} = \{0, 1, 2\}$, we have

$$\left(\sum_{x \in \mathcal{S}} |v_x| \right)^2 \leq 3 \sum_{x \in \mathcal{S}} v_x^2 = 3$$

by Jensens inequality, and consequently

$$\sum_{x, z \in \mathcal{S}, x \neq z} |v_x| |v_z| = \left(\sum_{x \in \mathcal{S}} |v_x| \right)^2 - \sum_{x \in \mathcal{S}} v_x^2 \leq 2. \quad (64)$$

We can thus establish

$$\begin{aligned} v^T M' v &= \sum_{x, z \in \mathcal{S}} v_x M'_{xz} v_z \\ &= \sum_{x \in \mathcal{S}} v_x M'_{xx} v_x + \sum_{x, z \in \mathcal{S}, x \neq z} v_x M'_{xz} v_z \\ &\geq \frac{2}{3} \sum_{x \in \mathcal{S}} v_x^2 - \frac{1}{3} \sum_{x, z \in \mathcal{S}, x \neq z} |v_x| |v_z| \\ &= 0, \end{aligned}$$

where we used that $M'_{xx} \geq 2/3$ and hence $M'_{xz} \leq 1/3$ for $x \neq z$, and applied inequality (64). This contradicts (63), which is why all eigenvalues must be positive. \square

Acknowledgments

This work was in part supported by the German Science Foundation (DFG) through grant CRC 755, projects A4 and A6, and the cluster of excellence “Multiscale Bioimaging: From Molecular Machines to Networks of Excitable Cells”. We are furthermore grateful to Mira Jürgens for computational assistance and proofreading.

References

- [1] T. Aspelmeier, A. Egner, and A. Munk. “Modern statistical challenges in high-resolution fluorescence microscopy”. In: *Annual Review of Statistics and Its Application* 2.1 (2015), pp. 163–202.
- [2] F. Balzarotti et al. “Nanometer resolution imaging and tracking of fluorescent molecules with minimal photon fluxes”. In: *Science* 355.6325 (2017), pp. 606–612.
- [3] S. Basu, R. Pollack, and M.-F. Coste-Roy. *Algorithms in real algebraic geometry*. Vol. 10. Springer Science & Business Media, 2007.

- [4] J. E. Berlier et al. “Quantitative comparison of long-wavelength Alexa Fluor dyes to Cy dyes: fluorescence of the dyes and their bioconjugates”. In: *Journal of Histochemistry & Cytochemistry* 51.12 (2003), pp. 1699–1712.
- [5] E. Betzig et al. “Imaging intracellular fluorescent proteins at nanometer resolution”. In: *Science* 313.5793 (2006), pp. 1642–1645.
- [6] M. Born and E. Wolf. *Principles of Optics*. 7th ed. Cambridge University Press, 1999.
- [7] R. M. Corless et al. “On the LambertW function”. In: *Advances in Computational Mathematics* 5.1 (1996), pp. 329–359.
- [8] A. Egner et al. “Fluorescence nanoscopy in whole cells by asynchronous localization of photoswitching emitters”. In: *Biophysical journal* 93.9 (2007), pp. 3285–3290.
- [9] W. Feller. *An Introduction to Probability Theory and its Applications*. Vol. 2. John Wiley & Sons, 2008.
- [10] J. Fölling et al. “Fluorescence nanoscopy by ground-state depletion and single-molecule return”. In: *Nature Methods* 5 (2008), pp. 943–945.
- [11] J. W. Goodman. *Introduction to Fourier Optics*. 2nd ed. New York: McGraw-Hill book company, inc., 1996.
- [12] P. Harremoës, O. Johnson, and I. Kontoyiannis. “Thinning, entropy, and the law of thin numbers”. In: *IEEE Transactions on Information Theory* 56.9 (2010), pp. 4228–4244.
- [13] S. W. Hell. “Microscopy and its focal switch”. In: *Nature methods* 6.1 (2008), p. 24.
- [14] S. W. Hell and J. Wichmann. “Breaking the diffraction resolution limit by stimulated emission: stimulated-emission-depletion fluorescence microscopy”. In: *Optics letters* 19.11 (1994), pp. 780–782.
- [15] S. W. Hell et al. “The 2015 super-resolution microscopy roadmap”. In: *Journal of Physics D: Applied Physics* 48.44 (2015), p. 443001.
- [16] S. T. Hess, T. P. Girirajan, and M. D. Mason. “Ultra-high resolution imaging by fluorescence photoactivation localization microscopy”. In: *Biophys J.* 91 (2006), pp. 4258–72.
- [17] M. Hirsch et al. “A stochastic model for electron multiplication charge-coupled devices – from theory to practice”. In: *PLoS ONE* 8.1 (2013), e53671.
- [18] J. Kemény and J. Snell. *Finite Markov Chains*. Van Nostrand, 1960.
- [19] O. Laitenberger et al. “Towards unbiased molecule counting in superresolution fluorescence microscopy”. Preprint (2019).
- [20] S.-H. Lee et al. “Counting single photoactivatable fluorescent molecules by photoactivated localization microscopy (PALM)”. In: *Proceedings of the National Academy of Sciences* 109.43 (2012), pp. 17436–17441.
- [21] T. C. Messina et al. “Hidden Markov model analysis of multichromophore photobleaching”. In: *The Journal of Physical Chemistry B* 110.33 (2006), pp. 16366–16376.
- [22] C. D. Meyer. *Matrix analysis and applied linear algebra*. Vol. 71. Siam, 2000.
- [23] B. Mityagin. “The zero set of a real analytic function”. In: *arXiv preprint arXiv:1512.07276* (2015).
- [24] L. Patel et al. “A hidden Markov model approach to characterizing the photo-switching behavior of fluorophores”. In: *bioRxiv* (2017), p. 223875.
- [25] M. S. Robbins and B. J. Hadwen. “The noise performance of electron multiplying charge-coupled devices”. In: *IEEE Transactions on Electron Devices* 50.5 (2003), pp. 1227–1232.

- [26] G. C. Rollins et al. “Stochastic approach to the molecular counting problem in superresolution microscopy”. In: *Proceedings of the National Academy of Sciences* 112.2 (2015), E110–E118.
- [27] M. J. Rust, M. Bates, and X. Zhuang. “Sub-diffraction-limit imaging by stochastic optical reconstruction microscopy (STORM)”. In: *Nature Methods* 3 (2006), pp. 793–796.
- [28] A. M. Sydor et al. “Super-resolution microscopy: from single molecules to supramolecular assemblies”. In: *Trends in cell biology* 25.12 (2015), pp. 730–748.
- [29] K. Tsekouras et al. “A novel method to accurately locate and count large numbers of steps by photobleaching”. In: *Molecular biology of the cell* 27.22 (2016), pp. 3601–3615.
- [30] S. Van de Linde et al. “Direct stochastic optical reconstruction microscopy with standard fluorescent probes”. In: *Nature protocols* 6.7 (2011), p. 991.
- [31] J. Vogelsang et al. “Make them blink: Probes for super-resolution microscopy”. In: *ChemPhysChem* 11.12 (2010), pp. 2475–2490.